Stratigraphic Analysis and Reservoir Characterization of the Late Oligocene – Early Miocene, Upper Yenimuhacir Group, Thrace Basin, Turkey

Ali Can Diyarbakirli

Thesis submitted to the faculty of the Virginia Polytechnic Institute and State University in partial fulfillment of the requirements for the degree of

Master of Science

In

Geosciences

Kenneth A. Eriksson, Co-Chair

Brian W. Romans, Co-Chair

Richard D. Law

December 5, 2016

Blacksburg, VA

Keywords: Thrace Basin, Hydrocarbon Potential, Reservoir Characterization.

Stratigraphic Analysis and Reservoir Characterization of the Late Oligocene – Early Miocene, Upper Yenimuhacir Group, Thrace Basin, Turkey

Ali Can Diyarbakirli

Abstract

The Thrace Basin, NW Turkey, is one of the most important basins in Turkey in terms of hydrocarbon potential. Previous studies, starting in the 1930s, focused on tectonics, basin evolution, sedimentation and stratigraphy, depositional systems, and hydrocarbon potential. Eocene turbiditic sandstones and reefal limestones, and Oligocene deltaic sandstones are the major reservoir targets in the basin today. The focus of this research is the Upper Oligocene deltaic sandstones, namely the Danismen and Osmancik formations, which contain potential hydrocarbon reservoirs. The aims of research were to develop a better understanding of the geometric configuration of the Oligocene strata and to identify potential reservoirs within the study area. Accordingly, the geometric configurations of the strata were delineated using 3D seismic reflection data whereas petro-physical properties of the target formations were determined using wireline logs from three wells. A right-lateral strike slip or reverse fault system and associated NW-SE trending asymmetric fold extend across the study area. Both the fault system and the fold are truncated beneath the Miocene unconformity and are thus dated as late Oligocene to early Miocene in age. The Miocene unconformity forms a stratigraphic trap whereas the fault system and associated fold construct a NW-SE trending structural trap. Hydrocarbon-bearing, five main clean sandstone (shale volume less than %10) intervals were identified using wireline logs and evaluated as potential targets. Hydrocarbon concentrations increase through the fold structure. Thus, the fault system and the associated asymmetric fold were the main factors that affected the zonal distribution of hydrocarbons in the study area.

Stratigraphic Analysis and Reservoir Characterization of the Late Oligocene – Early Miocene, Upper Yenimuhacir Group, Thrace Basin, Turkey

Ali Can Diyarbakirli

General Audience Abstract

Thrace Basin, northwest part of Turkey, is one of the most important basins in Turkey in terms of oil and gas potential. Previous studies started in1930s and included studies on the geology of the basin. Major reservoir targets in the basin today are Eocene turbiditic sandstones and reefal limestones, and Oligocene deltaic sandstones. This study focuses on the Oligocene deltaic sandstones of the Danismen and Osmancik formations, which are significant in terms of the oil and gas potential in the basin. The main purpose of this thesis is to evaluate the geometric configurations of these two formations and to identify potential reservoirs within the study area. For this purpose, geometric representation of the study area was generated by mapping the formations with the help of 3D seismic data. Reservoir characteristics related to physical properties were determined by utilizing the data obtained from three wells within the study area. As a result, potential reservoir zones are discovered mainly in the Danismen Formation, which can further be incorporated with exploration activities in the basin.

Acknowledgements

Firstly, I am greatly thankful to Dr. Kenneth A. Eriksson, my advisor. I am the most grateful for his support and guidance throughout this study.

I also would like to give my thanks to the committee members, Dr. Brian Romans and Dr. Richard Law. Their contributions were invaluable.

Additionally, I owe special thanks to the Turkish Petroleum Corporation, which provided the data set for this research and supported me throughout my education.

My family and my friends, thank you all so much for your support throughout my Master's years.

Table of Contents

List of Figures

List of Tables

1. Introduction

The Thrace Basin, NW Turkey, is one of the most important basins in Turkey in terms of hydrocarbon potential. The first commercial gas was discovered in 1970 by the Turkish Petroleum Corporation (TPAO) in the Hamitabat field, which is one of the largest gas fields in the basin. Since then, exploration and production activities have increased. Previous studies, starting in the 1930's, focused on tectonics, basin evolution, sedimentation and stratigraphy, depositional systems, and hydrocarbon potential (e.g. Yilmaz et al., 1995; Gorur & Okay, 1996; Turgut & Eseller, 2000; Coskun, 2000; Perincek et al., 2015). Eocene turbiditic sandstones and reefal limestones, and Oligocene deltaic sandstones are the major targets in the basin today.

3D seismic reflection surveys provide an opportunity to enhance the understanding of subsurface geologic features such as the stratigraphic and structural framework of the study interval, and the distribution and geometry of the potential source and reservoir strata, and structural and stratigraphic traps in a basin. Moreover, analysis of well logs provides information on the petro-physical properties of strata in a basin. Integration of seismic reflection and well data can decrease the uncertainties of interpretation of the hydrocarbon potential of prospective reservoirs.

This study utilizes 3D seismic reflection data and wireline logs from three wells provided by the Turkish Petroleum Corporation (TPAO) to investigate the stratal geometries and reservoir qualities of the Late Oligocene Upper Yenimuhacir Group, namely Danismen and Osmancik deltaic sandstones in the Thrace Basin (Figure 1.1) with a view to contributing to the exploration and production activities in the region. The 3D seismic reflection survey covers approximately 120 km^2 and is complemented by wireline logs from three wells within the seismic reflection survey that provide petro-physical properties of potential reservoir rocks (Figure 1.2).

Figure 1.1: Map showing the location of the Thrace Basin (retrieved from Google Earth).

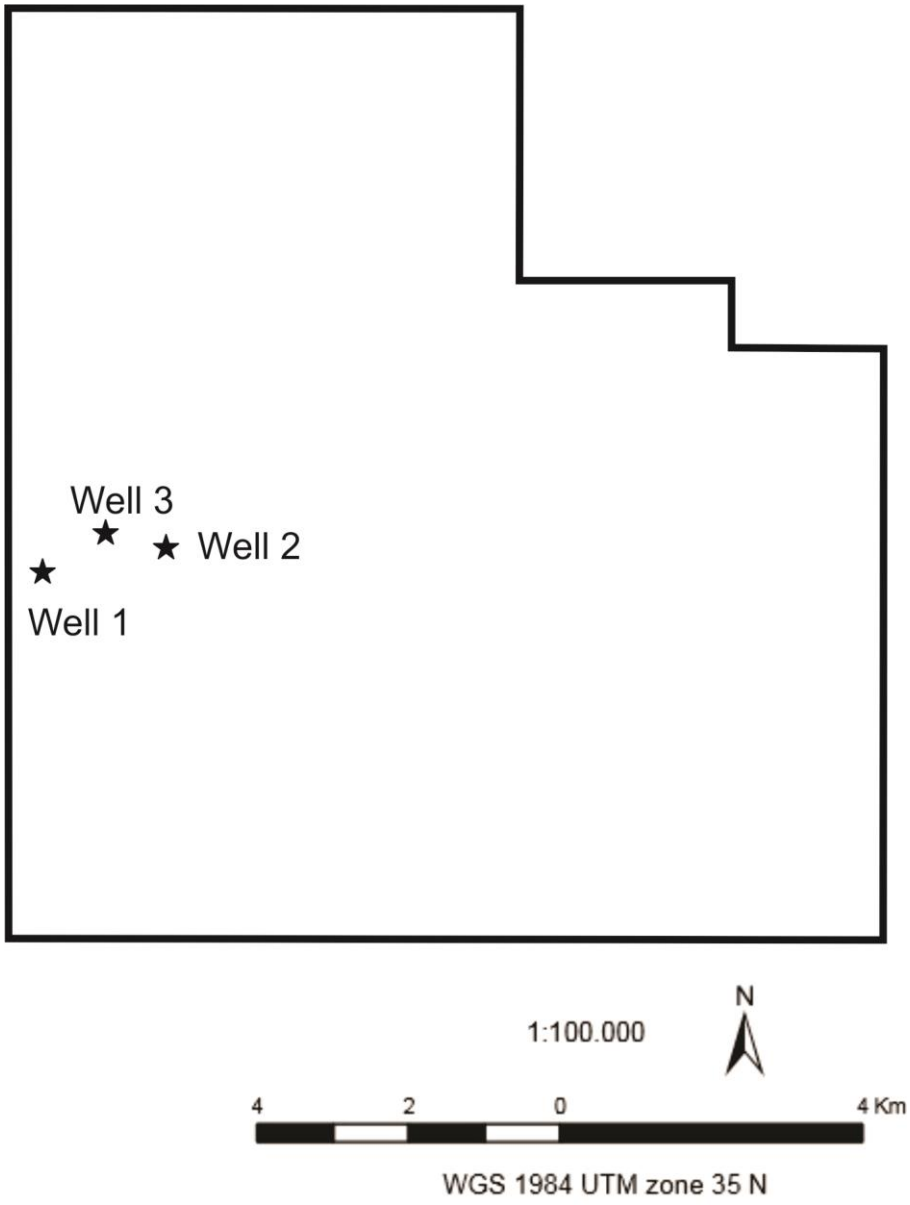

Figure 1.2: Data map showing the 3D seismic reflection survey area and well locations.

2. Geological Setting

Thrace Basin is a rectangular area covering approximately 1500 km^2. The basin fill underlain by Cenozoic basement which consists of different rock types. Rhodope and Strandja Massifs are located in the north, Istanbul Paleozoic sequences are located in the east and northeast, and the Sakarya continent represented by ophiolitic melange is located to the south and southeast of Thrace Basin (Figure 2.1) (Huvaz, Karahanoglu, & Ediger, 2007).

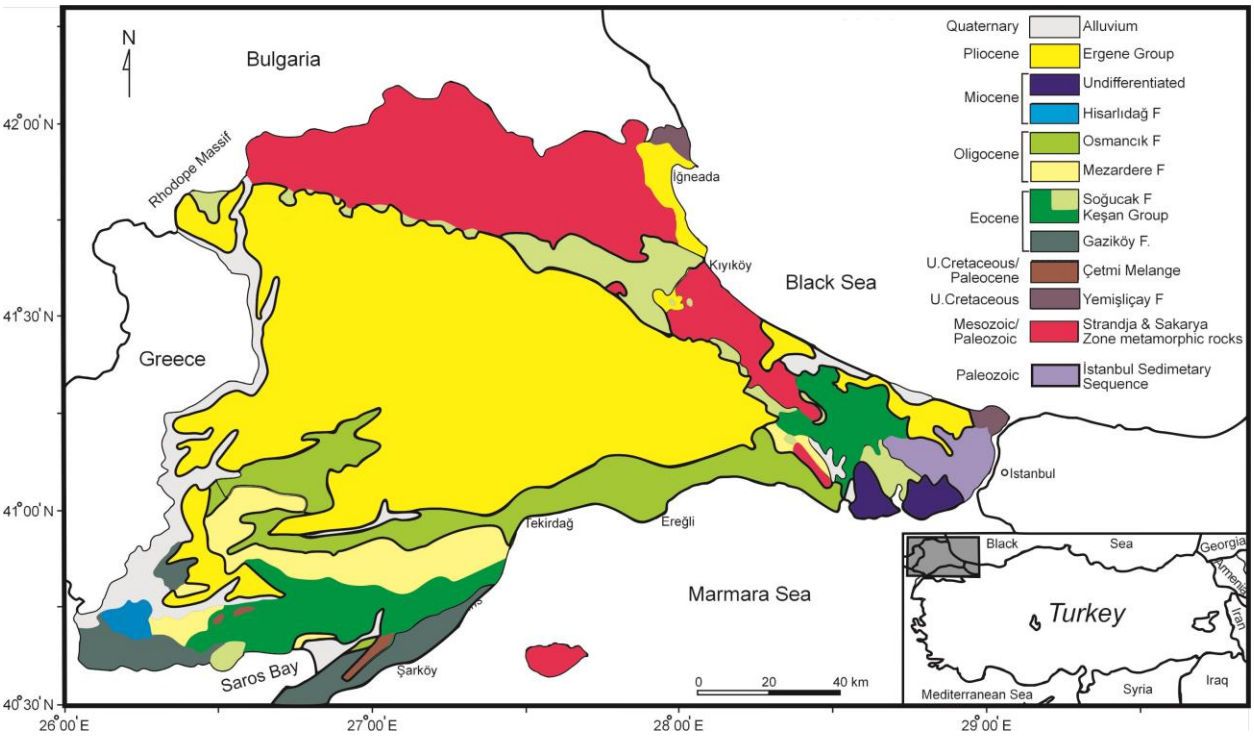

Figure 2.1: The geological map of the Thrace Basin (modified from Huvaz, Karahanoglu & Ediger 2007).

Thrace Basin has been interpreted as a remnant ocean basin (Yilmaz et al., 1995), a forearc basin (Gorur & Okay, 1996) and, more recently, as an intermontane basin (Coskun, 2000) or as a forearc that evolved into a intermontane basin (Siyako & Huvaz, 2007). The basin developed in the Late Cretaceous-Oligocene associated with the closure of the Intra-Pontide Ocean to the

south. This closure created a basin bounded by volcano-plutonic rock assemblages associated and metamorphic rocks of the Strandja Massif, and an accretionary mélange above the subducting Intra-Pondite Ocean. Depositional sequences of this time period are stratigraphically below Hamitabat and Gazikoy formations of this study (Siyako & Huvaz, 2007). Following closure of the ocean, the Thrace basin evolved into intermontane or remnant basin as a result of changes in the stress field that resulted in transpression (Siyako & Huvaz, 2007).

Sedimentation in Thrace Basin commenced in the Early Eocene and continued into the Pliocene (Figure 2.2). In the center of the basin, the sedimentary fill is up 9 km thick. Five depositional sequences separated by unconformities are recognizable in the basin (Fig. 2.2). The oldest sequence is characterized by clastic continental deposits whereas the second and third sequences consist of transgressive carbonate shelf overlain by progradational deltaic deposits. The fourth sequence is composed of continental red beds with local coal seams. The youngest sequence is made up of alluvial fan, fluvial channel and lagoonal deposits (Turgut & Eseller, 2000). The Danismen and Osmancik formations, the focus of this study, comprise the progradational component of sequence 3 (Fig. 2.2).

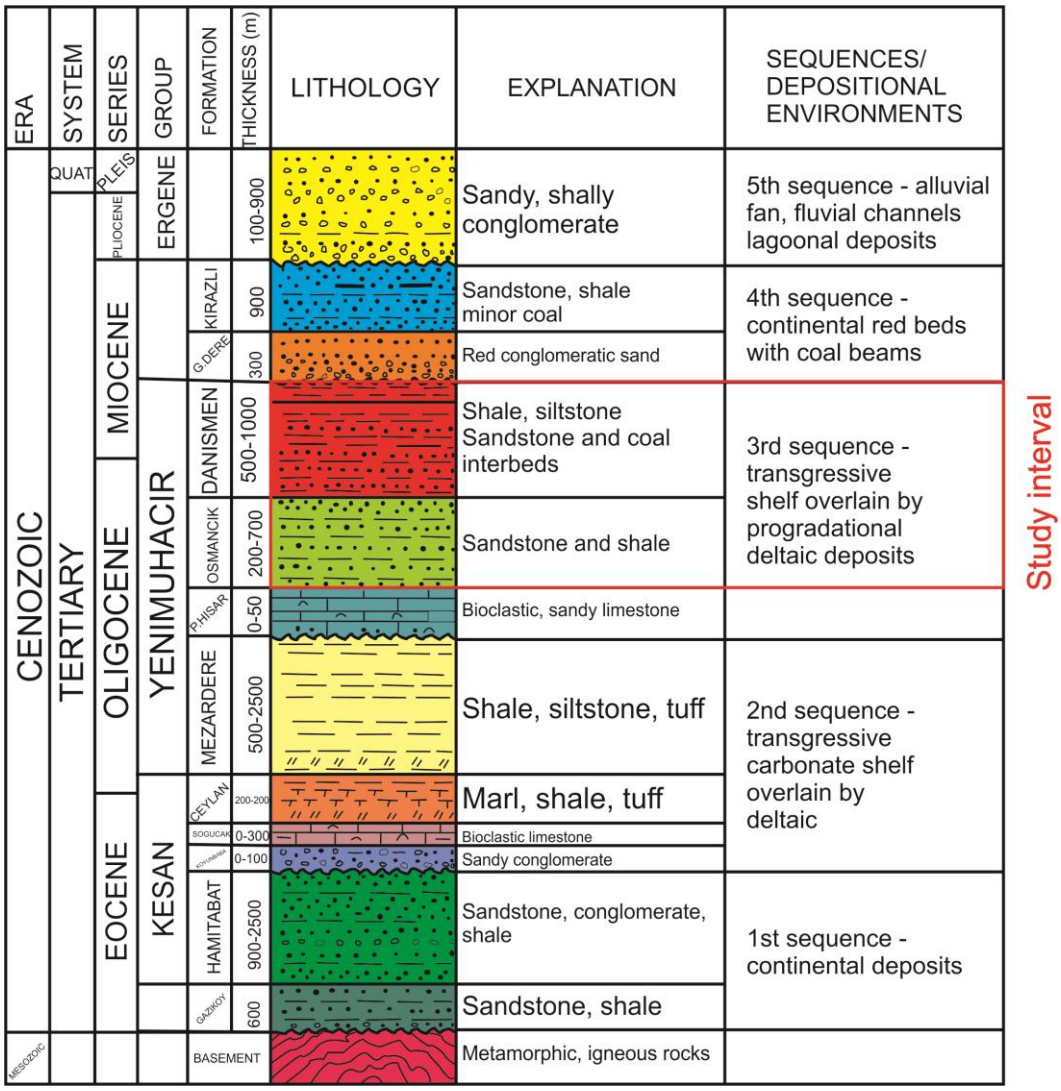

Figure 2.2: Stratigraphic column for the Thrace Basin (modified from Turgut and Eseller, 1999).

Prominent structural elements in this basin caused intense deformation in the south and north-northeast (Fig. 2.3). The North Anatolian Fault Zone (NAFZ), which extends for more than 1000 kilometers in an east-west direction across northern Turkey and reaches to the Sea of Marmara and the Aegean Sea at its westernmost extent, deformed the southern part of the Thrace Basin starting in Plio-Pleistocene and continuing up to present time with recent seismic activity along its extent (Turgut & Eseller, 2000). The Terzili Fault Zone (TFZ) was active probably starting in the late Early to Middle Miocene in the northern part of the basin and deformed all the

sedimentary deposits below Plio-Quarternary aged alluvial sedimentary cover in the northern half of the Thrace Basin (Fig. 2.3). Both the NAFZ and TFZ fault systems experienced lateral and reverse tectonic movements. As a consequence, deltaic Oligocene and Miocene sedimentary rocks are exposed in the southern part and crystalline basement rocks and Eocene marine sedimentary rocks are exposed on the northern part of Thrace Basin. Another prominent structure is a horst-like feature located in the east central part of Thrace Basin that provided accommodation for Eocene age reefal limestone deposits (Turgut & Eseller, 2000).

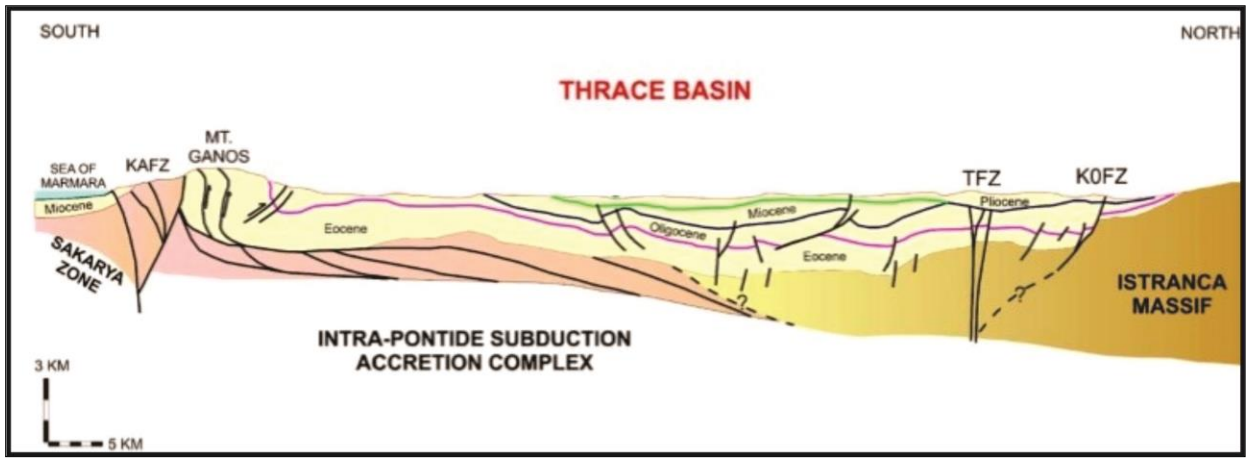

Figure 2.3: Cross-sectional view of the Thrace Basin (from Sunnetcioglu, 2008). KAFZ: North Anatolian Fault Zone, TFZ: Terzili Fault Zone, KOFZ: North Osmancik Fault Zone

Eocene reefal limestones and marine sandstones, and Oligocene-Early Miocene deltaic deposits, including the Danismen and Osmancik formations, are the best reservoir rocks in Thrace Basin. Non-marine alluvial deposits of Pliocene-Pleistocene age are potentially good reservoir rocks but seals are lacking (Turgut & Eseller, 2000). Late Eocene-Early Oligocene marine shales and marls are good source rocks.

2.1. Osmancik Formation

The Osmancik Formation is conformably underlain by the Pinarhisar Formation along the northern periphery of the Thrace Basin and by the Mezardere Formation in the basin center; it is overlain by the Danismen Formation (Turgut & Eseller, 2000). The Osmancik Formation is up 800 meters thick, consists of alternating sandstone, shale and, locally, limestones and tuff and displays an overall upward-coarsening in grain size (Perincek et al., 2015). Sedimentary facies record progradation of marine shelf to prodelta to delta-front settings. Based on palynological studies, an Early-Late Oligocene age is assigned to the Osmancik Formation (Perincek et al., 2015).

2.2. Danismen Formation

The Danismen Formation comformably overlies the Osmancik Formation and is deeply eroded beneath an unconformity that separates it from the overlying Ergene Group. The thickness of this formation is approximately 1000 meters and it is made up of sandstone, shale, conglomerate and coals that are assigned to lacustrine, swamp, fluvial and floodplain settings. Fish fossils and silicified wood are the characteristic features of the Danismen Formation (Perincek et al., 2015). The Danismen Formation is the uppermost unit of the prograding delta system and is interpeted as a delta-plain succession (Perincek et al., 2015). The Danismen Formation has been assigned ages of Early Oligocene (Sarac, 1987), Late Oligocene (Kasar & Eren, 1986; Bati et al., 2002), and Late Oligocene-Early Miocene (Alisan, 1985; Gerhard & Alisan, 1987; Bati et al., 1993) on the basis of paleontological studies including palynomorph and vertebrate fossils.

3. Methods

Data for this project were provided by the Turkish Petroleum Corporation and include a 3D seismic reflection survey, which covers approximately 120 km^2, and well log data from three wells in the study area. The Kingdom Suite software was utilized to analyze the seismic reflection and well data.

3.1. Seismic Data Interpretation

In general, the seismic reflection data workflow includes acquisition, processing, and interpretation steps. The seismic reflection survey for the study area had already been acquired and processed by the Turkish Petroleum Corporation. Post-stacked Time Migrated data were provided and the Kingdom Suite Interpretation software was used to analyze the seismic reflection data. Table 3.1 shows the acquisition parameters for the 3D seismic volume. Five prominent horizons were defined based on high amplitude, continuous reflections and differentiation in seismic facies. Moreover, a fault system in the seismic volume was distinguished. Therefore, a comprehensive subsurface geometry of the study area was delineated.

Table 3.1: Acquisition parameters for the 3D seismic reflection survey.

Record Length	5 sec
Sample Interval	0.02 sec
Dominant Frequency	20-30 Hz
Near-offset	35 m
Far-offset	3385 m
Fold	24
Bin Size	25 x 25
Receiver Spacing	50 m
Shotpoint Spacing	50 m
3D data obtained in rectangular grid	N-S inlines / E-W crosslines
Source	Explosion (Dynamite)

Attempts were made to tie well logs to seismic data to produce a proper time/depth conversion. Unfortunately, well-tie attempts failed due to significant uncertainty in the correlation between the seismic and synthetic traces. Therefore, all of the seismic maps in this study were generated in the time domain.

Furthermore, the Danismen and Osmancik formations were identified and mapped in the seismic space. In this regard, time-structure contour and isochron (thickness) maps were produced for both formations. Time-structure contour maps are maps in seismic time (depth) at which stratal surfaces are located. Time-structure contour maps in the time domain were prepared for the tops of the Danismen and Osmancik formations. Isochron maps show the variations in the difference of two way travel times between two seismic reflections. Thickness changes of the Danismen and Osmancik formations were mapped across the seismic volume in the time domain using the formation boundary horizons.

3.2. Well Log Data Interpretation

Wireline logs provided from the three wells are listed in Table 3.2. Log analysis is explained in the following sections.

Table 3.2: Log types and their utilities

Log Types	**Explanation**
Resistivity Logs (LLD, LLS, MSFL)	Differentiation of hydrocarbons from water
Gamma Ray	Identification of lithologies and permeable zones
Spontaneous Potential	Determination of gross lithology and shale volume
Density	Porosity determination and gas presence
Neutron	Porosity determination and gas presence
Sonic	Porosity determination and P-wave

(Asquith & Krygowski, 2004)

3.2.1. Porosity Logs

Density and Neutron logs were used to calculate porosity values and determine the gas-bearing zones in the study area. Density logs, which measure the bulk density of the lithology, are used to calculate density derived porosity (DPHI). The equation 3.1 was used to calculate density porosity (Asquith & Krygowski, 2004).

$$\phi = \frac{\rho ma - \rho b}{\rho ma - \rho fl} \qquad 3.1$$

where:

ϕ = Density derived porosity

ρ_{ma} = matrix density (2.644 g/cm^3 for sandstone)

ρ_b = formation bulk density

ρ_{fl} = fluid density (1 gr/cm^3 for fresh water)

Neutron logs measure the hydrogen concentration in a formation. In a shale-free formation, neutron log measures the liquid filled porosity (NPHI) (Asquith & Krygowski, 2004). Whenever a gas-bearing zone is present, neutron log porosity is lower than the actual formation porosity. Similarly, whenever clays are present in a formation, neutron porosity is greater than the actual porosity because of the higher hydrogen concentration in the clay-bearing formation (Asquith & Krygowski, 2004). Therefore, density and neutron derived porosities are combined together to calculate an average porosity (PHIT). The equation 3.2 was used to calculate the average porosity.

$$\Phi = \frac{\phi D + \phi N}{2} \qquad 3.2$$

where:

ϕ = Average porosity

ϕN = Neutron porosity

ϕD = Density porosity

Additionally, the crossover of the density and neutron log curves indicate gas presence in the formation. The greater the crossover between density and neutron log curves, the better the reservoir quality (Asquith & Krygowski, 2004).

Moreover, in shaly formations, porosity logs should be corrected for shale effects. Once volume of shale is determined, neutron and density logs can be corrected for shale effects. In this study, equations 3.3 and 3.4, Dewan (1983) formula for shale effect, were used:

$$\phi Ne = \phi N - Vsh \times \phi Nsh \qquad 3.3$$

where:

ϕNe = shale-corrected neutron porosity

ϕN = neutron porosity

Vsh = volume of shale

ϕNsh = neutron porosity of a nearby shale

$$\phi De = \phi D - Vsh \times \phi Dsh \qquad 3.4$$

where:

ϕDe = shale-corrected density porosity

ϕD = density porosity

Vsh = volume of shale

ϕDsh = density porosity of a nearby shale

After determining the shale-corrected porosities, a total effective porosity was produced with the Equation 3.5 below:

$$\phi E = \sqrt{\frac{\phi Ne^2 + \phi De^2}{2}} \quad 3.5$$

where:

ϕE = effective porosity

ϕDe = shale-corrected density porosity

ϕNe = shale-corrected neutron porosity

3.2.2. Shale Volume Determination

Shale volumes in the Danismen and Osmancik formations were calculated by using Gamma Ray logs. Both linear and nonlinear equations were used to determine shale volume in the formations (Asquith & Krygowski, 2004). The equations used are given below:

Linear relationship:

$$IGR = \frac{GRlog - GRmin}{GRmax - GRmin} \quad 3.6$$

where:

IGR = Gamma Ray Index,

GRmin = minimum gamma ray (clean sand or carbonate),

GRmax = maximum gamma ray (shale),

GRlog = gamma ray reading

For Tertiary rocks (Larionov, 1969):

$$Vsh = 0.083(2^{3.7 \times Igr} - 1) \quad 3.7$$

where:

Vsh = shale volume,

IGR = gamma ray index

Other equations for calculating Vsh are from:

Steiber (1970):

$$Vsh = \frac{Igr}{3 - 2 \times Igr} \quad 3.8$$

Clavier (1971):

$$Vsh = 1.7 - \sqrt{3.38 - (Igr - 0.7)^2} \quad 3.9$$

3.2.3. Archie Water Saturation and Bulk Volume Water

Water saturation is the ratio of water volume to pore volume. Water saturation (Sw) can be determined by using the Archie (1942) formula (Asquith & Krygowski, 2004):

$$Sw = \sqrt[n]{\frac{a \times Rw}{Rt \times \phi^{m}}} \qquad 3.10$$

where:

Sw = water saturation of the uninvaded zone

Rw = resistivity of formation water at formation temperature

Rt = true formation resistivity

ϕ = porosity

a = tortuosity factor

m = cementation exponent

n = saturation exponent

Since water resistivity (Rw) is not known, Pickett plots (Pickett, 1966, 1973) are used to estimate the water resistivity (Rw) and water saturation (Sw) values. The Pickett plot method is a graphical solution to Archie's equation for water saturation and is useful when the true resistivity of the formation (Rt) and the porosity are known. Rt is calculated by using the deep resistivity log curve (LLD) and is corrected for temperature with the equation 3.11. For formation temperature calculation, the thermal gradient is assumed to be 34.7^{o}C/km (Huvaz et al., 2007).

$$Rt = \frac{LLD \times (Temp + 21)}{(Tf + 21)} \quad 3.11$$

where:

Rt = resistivity at formation temperature

LLD = deep resistivity log reading

Temp = temperature at which resistivity was measured (surface temperature 20^{o}C is assumed)

Tf = formation temperature

Bulk volume water (BVW) is another important parameter to evaluate a reservoir since it indicates whether or not water is irreducible in a hydrocarbon-bearing zone. It is a product of water saturation and porosity. It is calculated with the equation 3.12.

$$BVW = Sw \times \phi \quad 3.12$$

where:

BVW = Bulk Volume Water

Sw = water saturation of an uninvaded zone

ϕ = porosity

3.2.4. Quick Look Methods

Apparent water resistivity (Rwa) and the Rxo/Rt (the ratio of deep and shallow resistivity readings) and wet resistivity (Ro) methods were applied to determine possible hydrocarbon zones in the strata. The Rxo/Rt method is a comparison of resistivity techniques that are plotted

as a curve on the log. Interpretation of the ratio relies on the observation of the log patterns along with the SP log. For shale, the ratio is relatively constant close to 1 and is comparable to the SP log curve. In water-bearing zones, the ratio follows the SP curve. In hydrocarbon-bearing zones, the ratio moves away from the SP curve (Asquith & Krygowski, 2004). On the other hand, the apparent water resistivity method depends on the calculation of water resistivity between intervals in a well. The basis for this technique is that the lowest of Rwa is the closest approximation to the true water resistivity (Rw), and the zone is most likely to be a water-bearing zone. Zones with greater Rwa values are probably hydrocarbon-bearing zones. By comparing different intervals in a well, hydrocarbon-bearing zones can be detected by this method (Asquith & Krygowski, 2004). Rwa is calculated using the equation 3.13:

$$Rwa = \frac{Rt \times \phi^{m}}{a} \qquad 3.13$$

where:

Rwa = apparent water resistivity

Rt = formation resistivity

ϕ = porosity

m = cementation exponent

a = tortuosity factor

The wet resistivity (Ro) method is another technique to determine possible hydrocarbon-bearing zones based on the comparison with formation resistivity curve. Simply, in water-bearing zones, both wet resistivity and formation resistivity curves should overlay whereas in hydrocarbon-

bearing zones formation resistivity values should be higher than wet resistivity values and the degree of the separation indicates the amount of hydrocarbon saturation. Wet resistivity (Ro) is calculated with the equation 3.14:

$$Ro = F \times Rw = \frac{a \times Rw}{\phi^m} \qquad 3.14$$

where:

Ro = wet resistivity

F = formation factor

Rw = water resistivity

a = tortuosity factor

m = cementation exponent

ϕ = porosity

4. Results

4.1. Seismic Data Analysis

The subsurface geometry of the study area is delineated from the interpretation of 3D seismic reflection data. Prominent horizons are identified based on high amplitude, continuous reflections that separate different seismic facies in the study area. Representative cross-sections from the study area (Figs. 4.1, 4.2, 4.3 and 4.4) show the uninterpreted data that indicate differences in resolution and changes in amplitude with depth. The stratigraphic succession of interest can be subdivided into three intervals of characteristic seismic reflection geometry: (1) an upper interval of horizontal, parallel reflections; (2) a middle interval showing large-scale mounded to wavy reflection geometries, which is interpreted as a fold structure; and (3) a lower interval of horizontal, parallel reflections. Figure 4.5 displays a perspective view of the area demonstrating the geometric variations of the reflection patterns and the extension of the deformation structure.

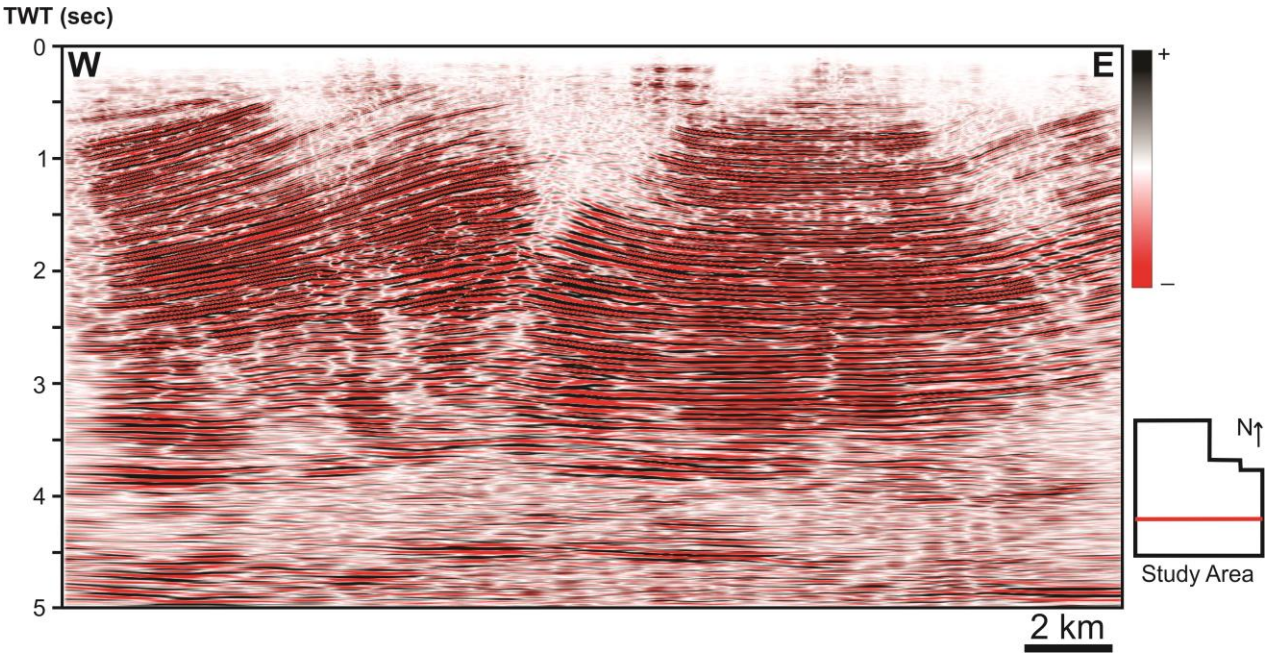

Figure 4.1: East-West oriented seismic cross section through the southern part of the study area showing the uninterpreted data. Note the low resolution in the lower part and the higher resolution in the upper part of the profile. Also note fold structure towards the top left of the profile.

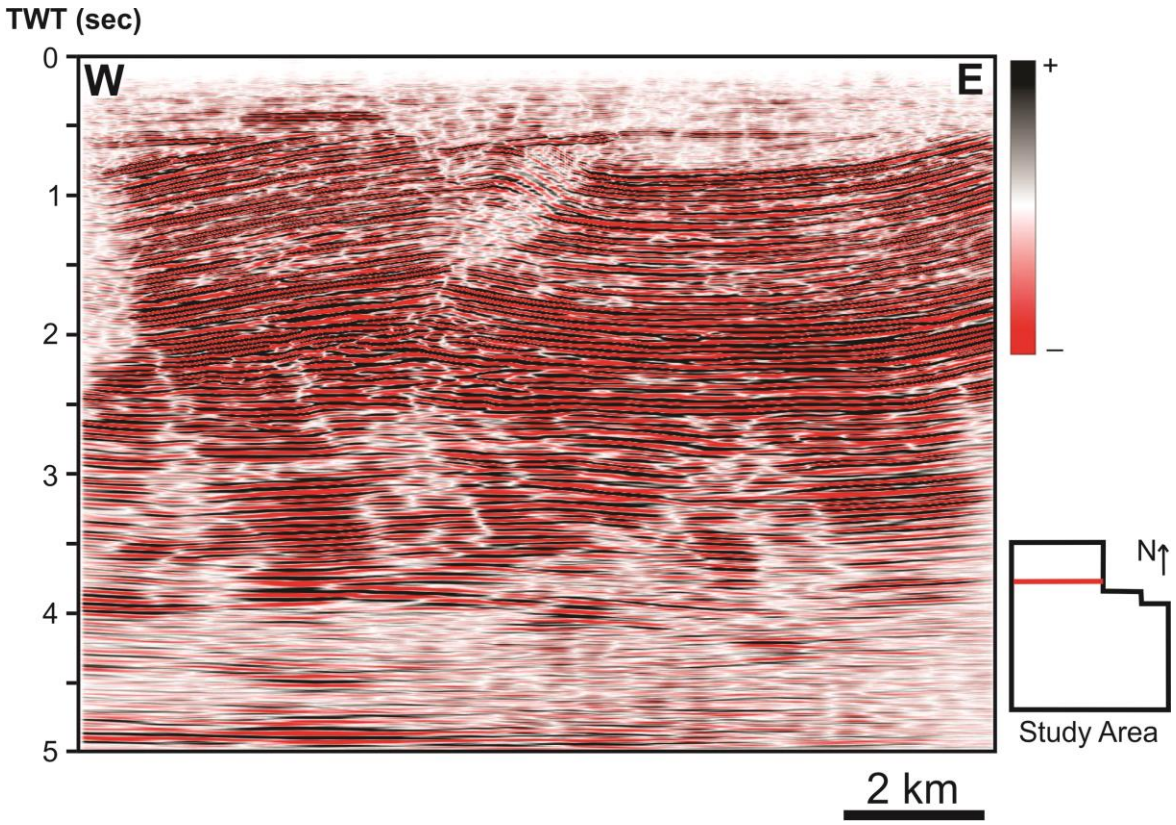

Figure 4.2: East-West oriented seismic cross section through the northern part of the study area showing the uninterpreted data. Note the low resolution in the lower part and the higher resolution in the upper part of the profile. Also note fold structure towards the top of the profile and the angular discontinuity in the top left of the profile.

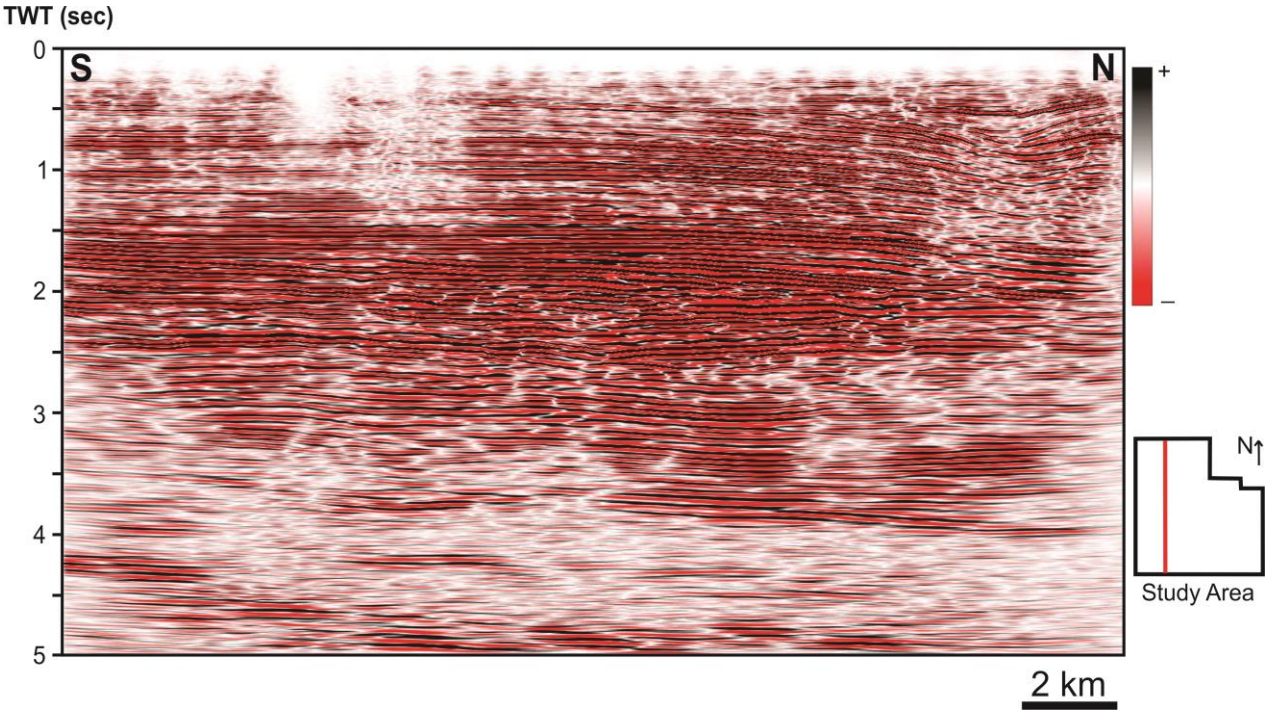

Figure 4.3: North-South oriented seismic cross section through the western part of the study area showing the uninterpreted data. Note the low resolution in the lower part and the higher resolution in the upper part of the profile.

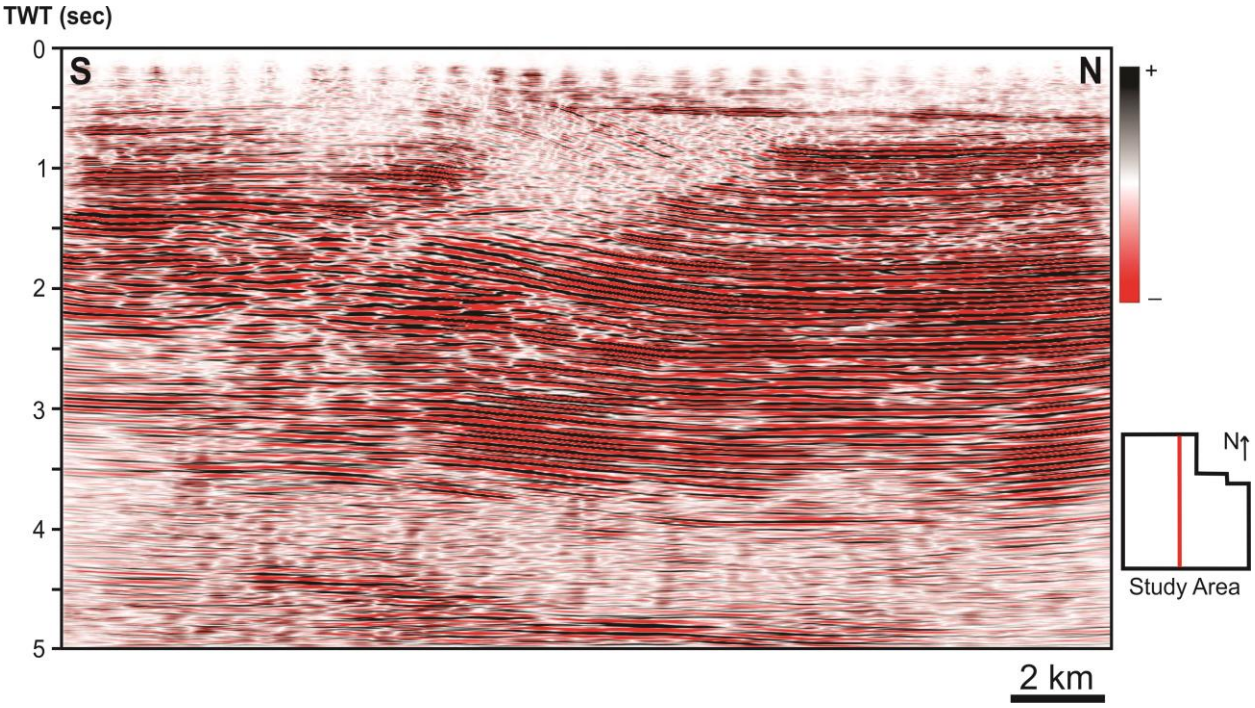

Figure 4.4: North-South oriented seismic cross section through the central part of the study area showing the uninterpreted data. Note the low resolution in the lower part and the higher resolution in the upper part of the profile. Also note fold structure towards the top of the profile.

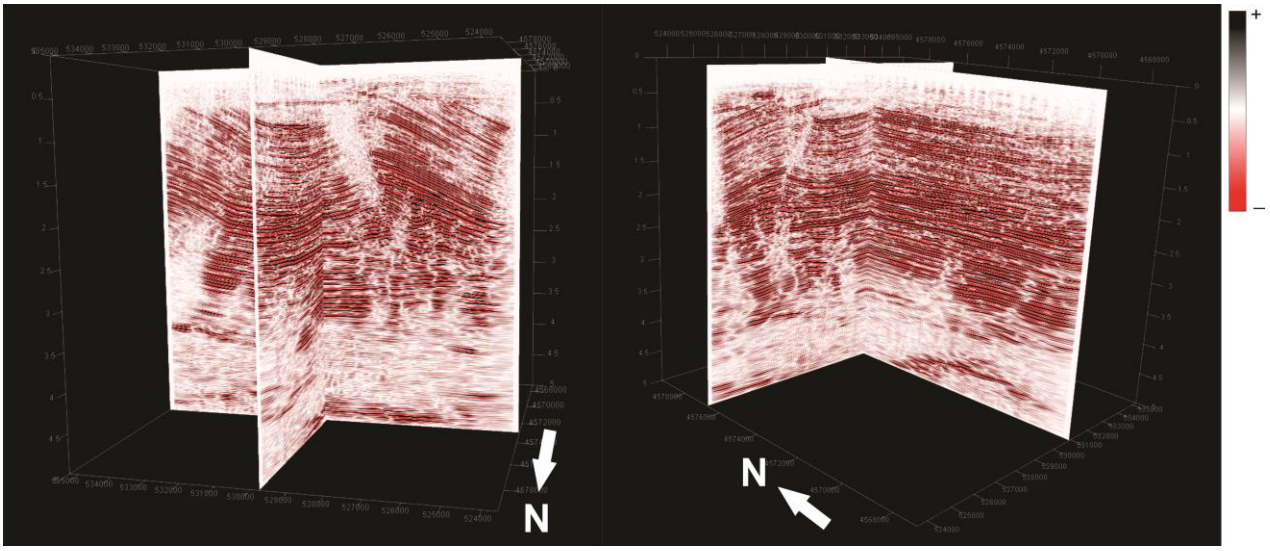

Figure 4.5: 3D perspective view of the study area showing the uninterpreted data. Note the major fold structure.

Target formations are defined and their stratal distributions in the study area determined within the 3D seismic volume. These are displayed in representative cross-sectional views of the Danismen and Osmancik formations (Figs. 4.6, 4.7, 4.8 and 4.9). The profiles show a major unconformity around 0.4-0.5 seconds TWT which also represents the top of the Danismen Formation. Beneath this erosional surface, wavy reflections characterize the Danismen and Osmancik formations between roughly 0.5-2.5 seconds TWT and are underlain and overlain by horizontal reflections (Figs. 4.6, 4.7, 4.8 and 4.9). A fold structure related to a local fault system exists within these strata between 0.5 and 2.0 seconds. The fault zone and steeply dipping limbs of the fold are lack of seismic response due to the steep surfaces. The horizontal strata between 2.5-5 seconds TWT are assumed to represent the underlying Mezardere Formation (Fig. 2.2). Stratal surfaces and their geometric extensions in three-dimensional space (Figs. 4.10, 4.11 and 4.12) also demonstrate that Danismen and Osmancik formations are characterized by wavy reflections bounded above and below by relatively horizontal reflections. In addition, these 3D perspectives indicate that the fold axis trends northwest-southeast, that the fold plunges to the northwest and that the fold is characterized by a gently dipping southwesterly limb and a steeply dipping northeasterly limb (Fig. 4.10 and 4.11). A perspective view of the fault in three dimensional space demonstrates the geometry of the asymmetric fold and the associated fault system and illustrates that these structures are located within the interval characterized by wavy reflections with quite low amplitude (Fig. 4.13). The fold and fault system are truncated beneath the Miocene unconformity. Because of the significant uncertainty of the time-depth conversions, time-structure contour maps and isochron maps for the target formations are shown in the time domain (Figs. 4.14, 4.15, 4.16 and 4.17). The top surface of the Danismen Formation is subhorizontal with local deepening in the northwest and shallowing over the fold (Fig. 4.14). The

top surface of the Osmancik Formation is shallowest over the fold and deepens east and west of the fold (Fig. 4.15). The fold plunges to the northwest and the eastern limb of the anticline ascends in the east of the study area. An isochron map of the Danismen Formation shows thinning over the fold and in the east, and thickening to the east and west (Fig. 4.16). The Osmancik Formation thickens over the fold and thins to the east and west (Fig. 4.17).

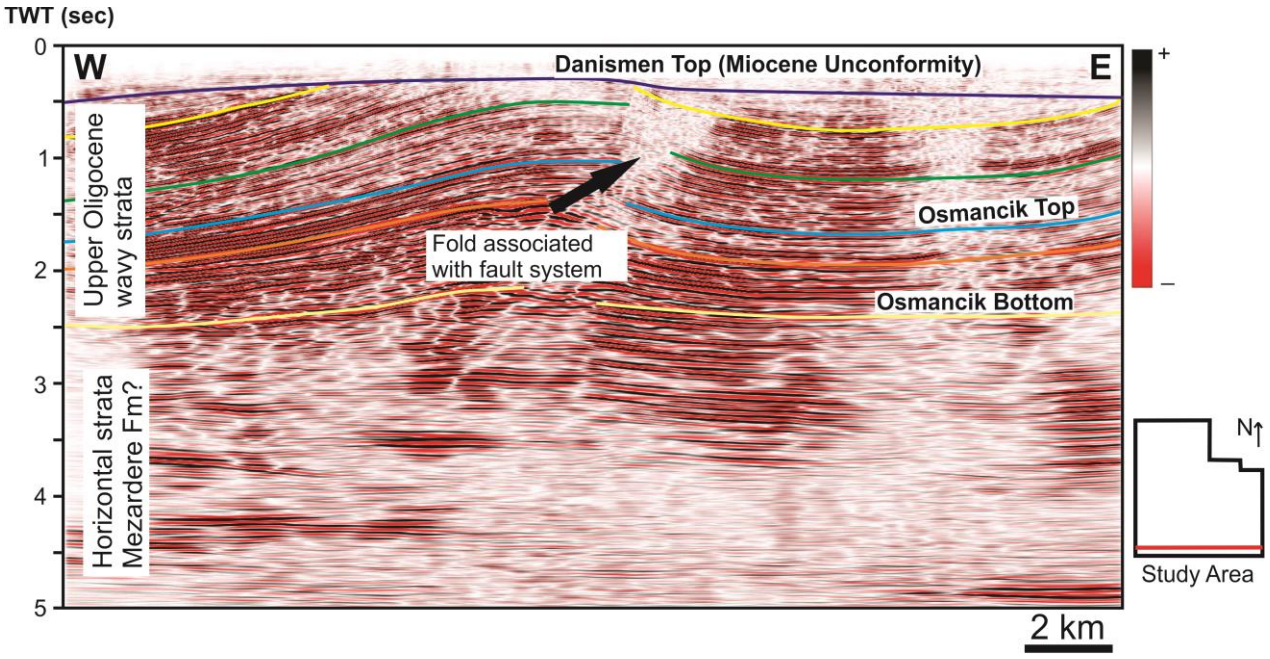

Figure 4.6: East-West oriented cross-sectional view of the study area with annotations showing selected horizons, formation boundaries and the Miocene-Oligocene boundary annotated. Note the fold structure associated with a reverse fault system in the upper half of the profile beneath the unconformity.

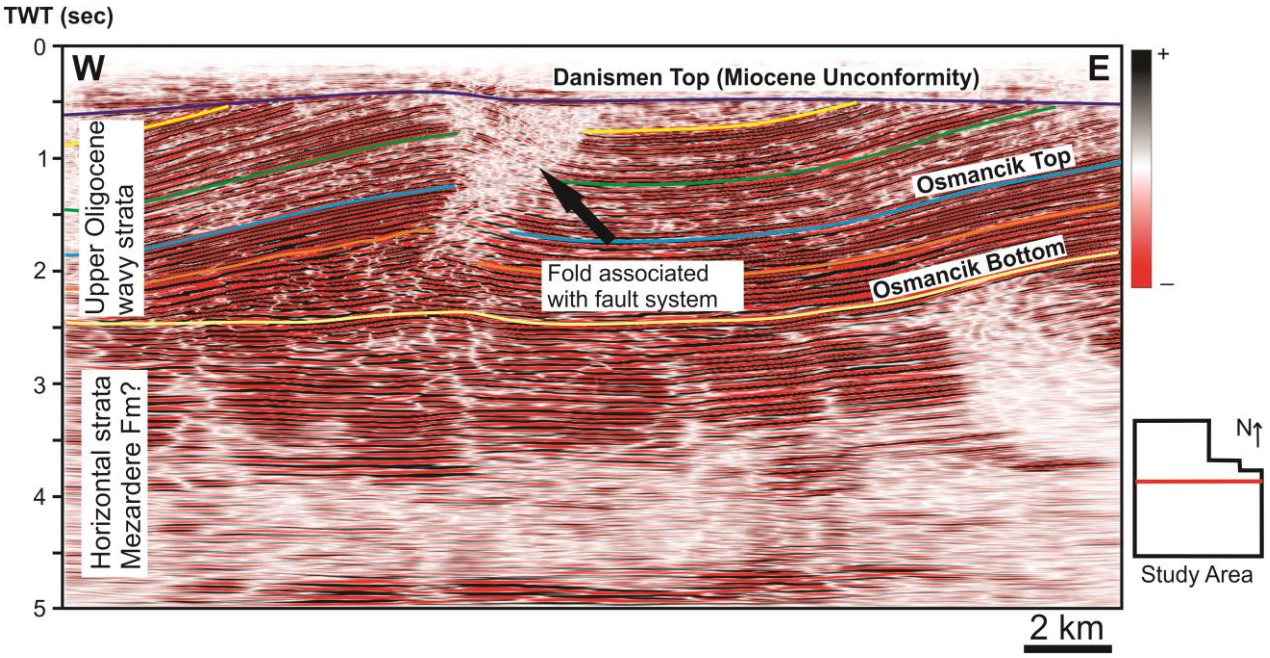

Figure 4.7: East-West oriented seismic cross section through the center of the study area showing selected horizons, formation boundaries and the Miocene-Oligocene boundary annotated. Note the fold structure associated with a reverse fault system in the upper half of the profile beneath the unconformity.

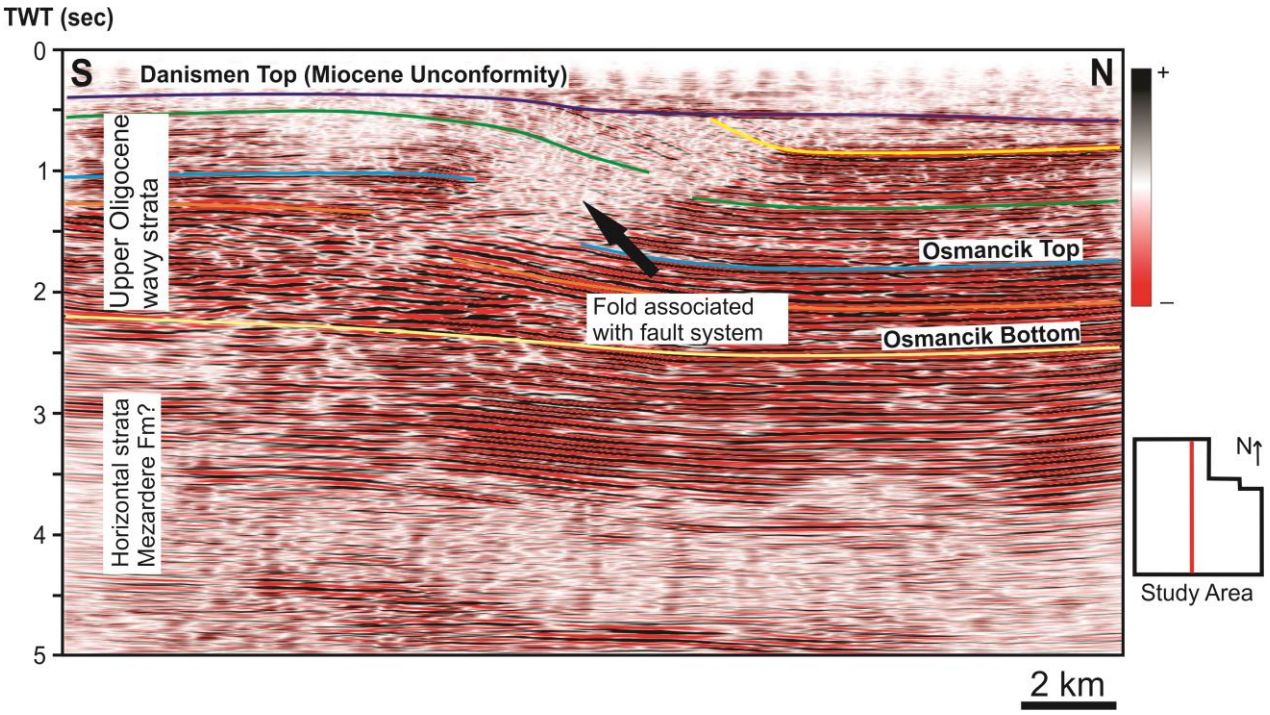

Figure 4.8: North-South oriented cross section through the central part of the study area showing selected horizons, formation boundaries and the Miocene-Oligocene boundary annotated. Note the fold structure associated with a reverse fault system in the upper half of the profile beneath the unconformity.

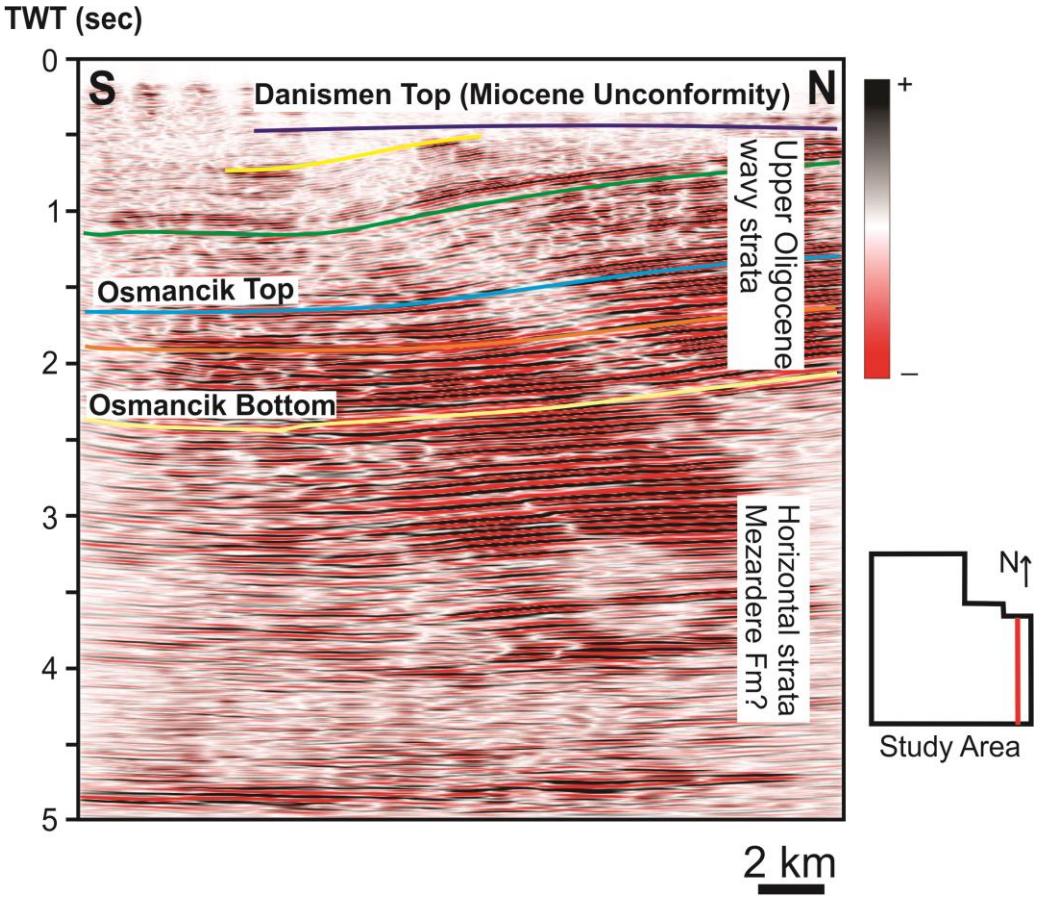

Figure 4.9: North-South oriented cross section through the eastern part of the study area showing selected horizons, formation boundaries and the Miocene-Oligocene boundary annotated. Note the steeper dip of the strata beneath the unconformity.

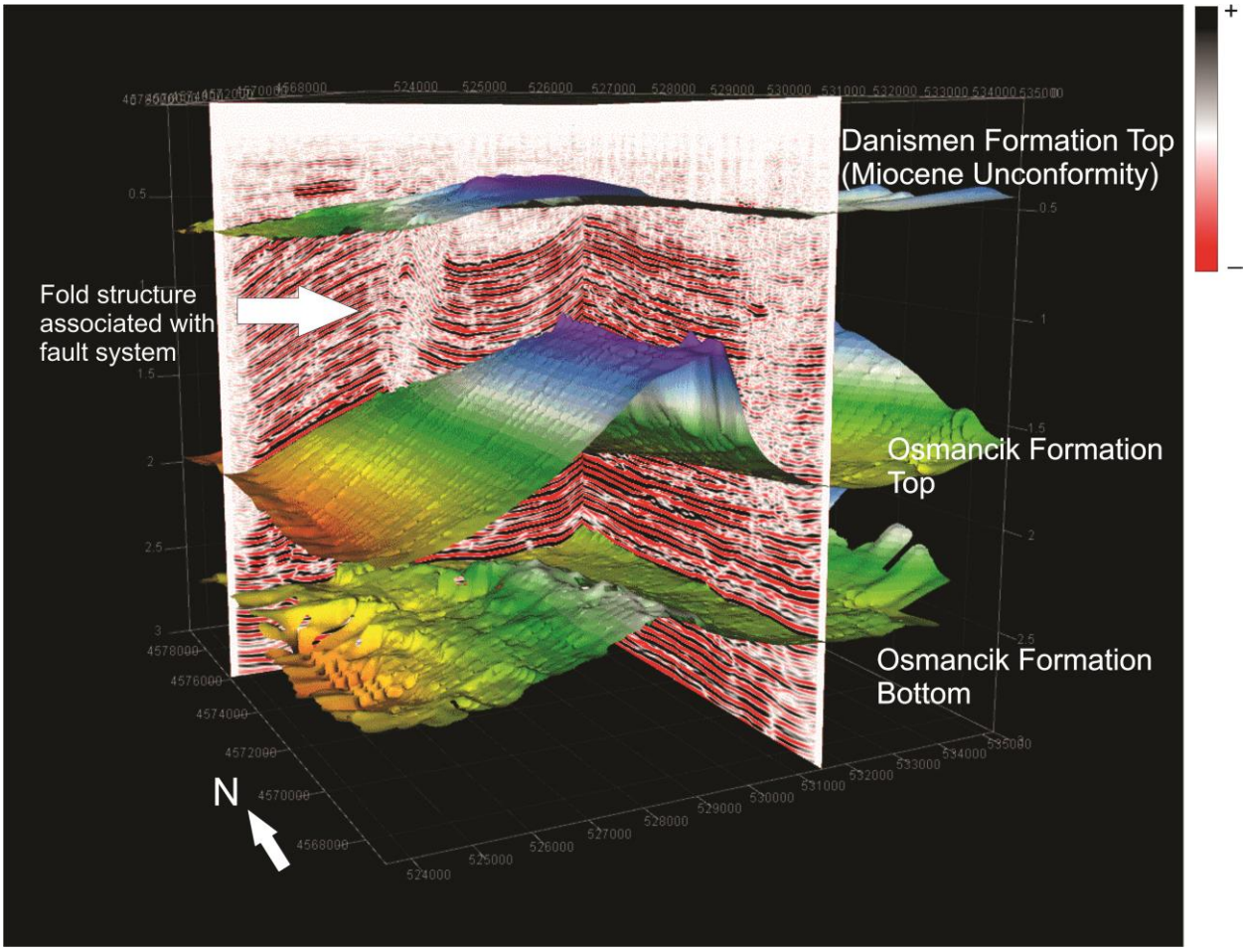

Figure 4.10: 3D perspective view of the study area (view from the southwest) showing formation base and top of the Osmancik and Danismen formations and the angular unconformity at the base of the Miocene. Note the northwest-southeast trend of the fold axis of the anticlinal structure associated with a reverse fault system and the truncation of the fold beneath the unconformity.

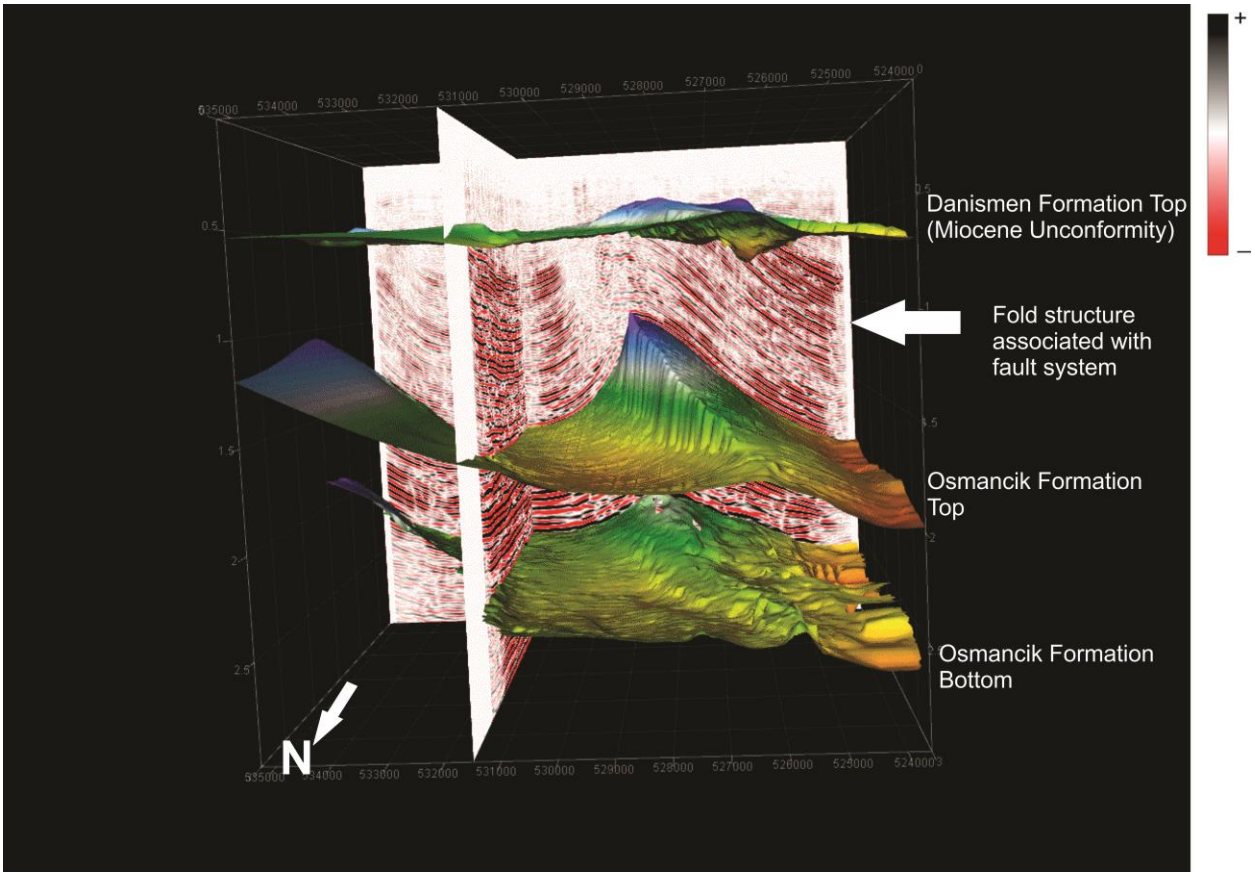

Figure 4.11: 3D perspective view of the study area (view from the north) showing formation base and top of the Osmancik and Danismen formations and the angular unconformity at the base of the Miocene. Note the northwest-southeast trend of the fold axis of the anticlinal structure, the plunge of the fold to the northwest and the truncation of the fold beneath the unconformity.

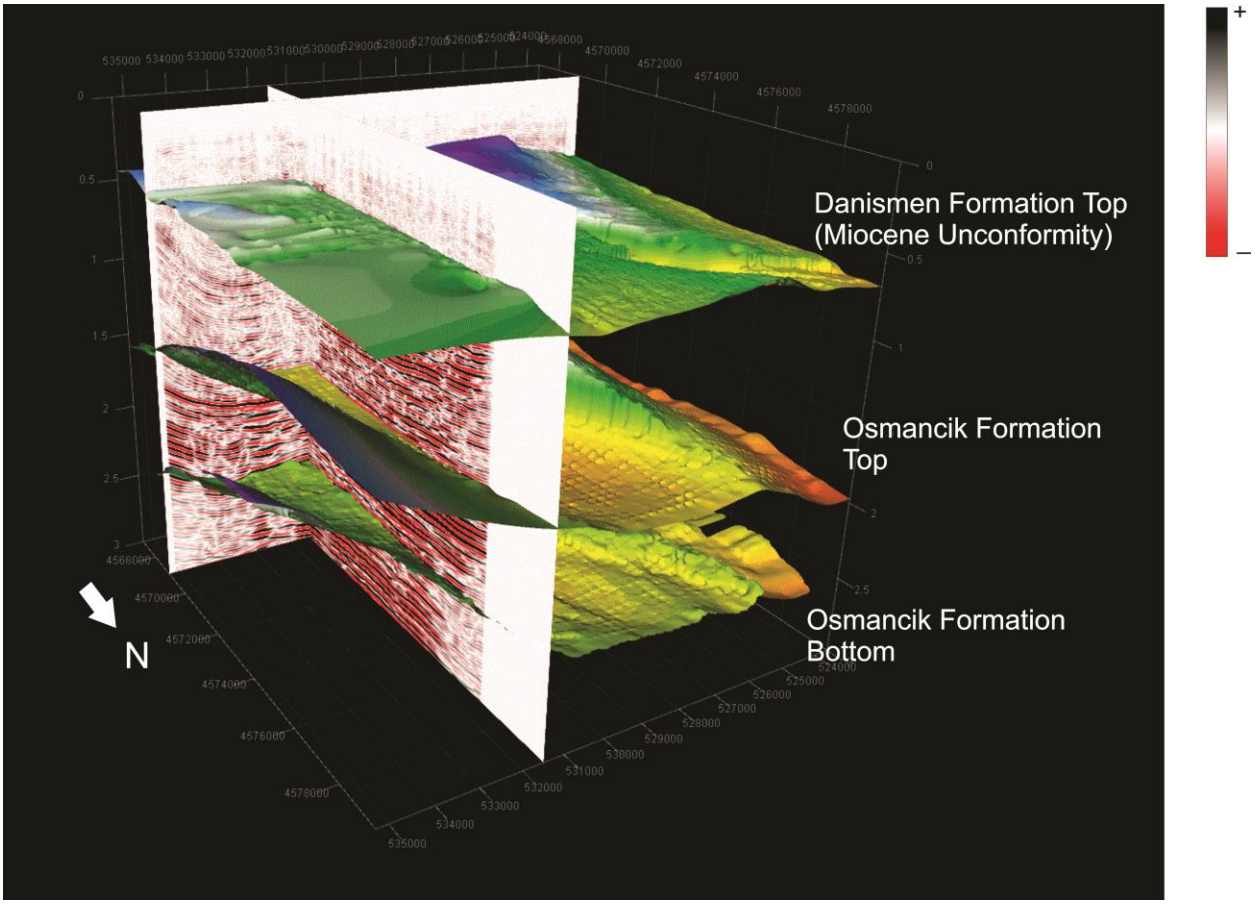

Figure 4.12: 3D perspective view of the study area (view from the northeast) showing formation base and top of the Osmancik and Danismen formations and the angular unconformity at the base of the Miocene. Note the rise of the east flank of the fold to the northeast and the truncation of the fold beneath the unconformity.

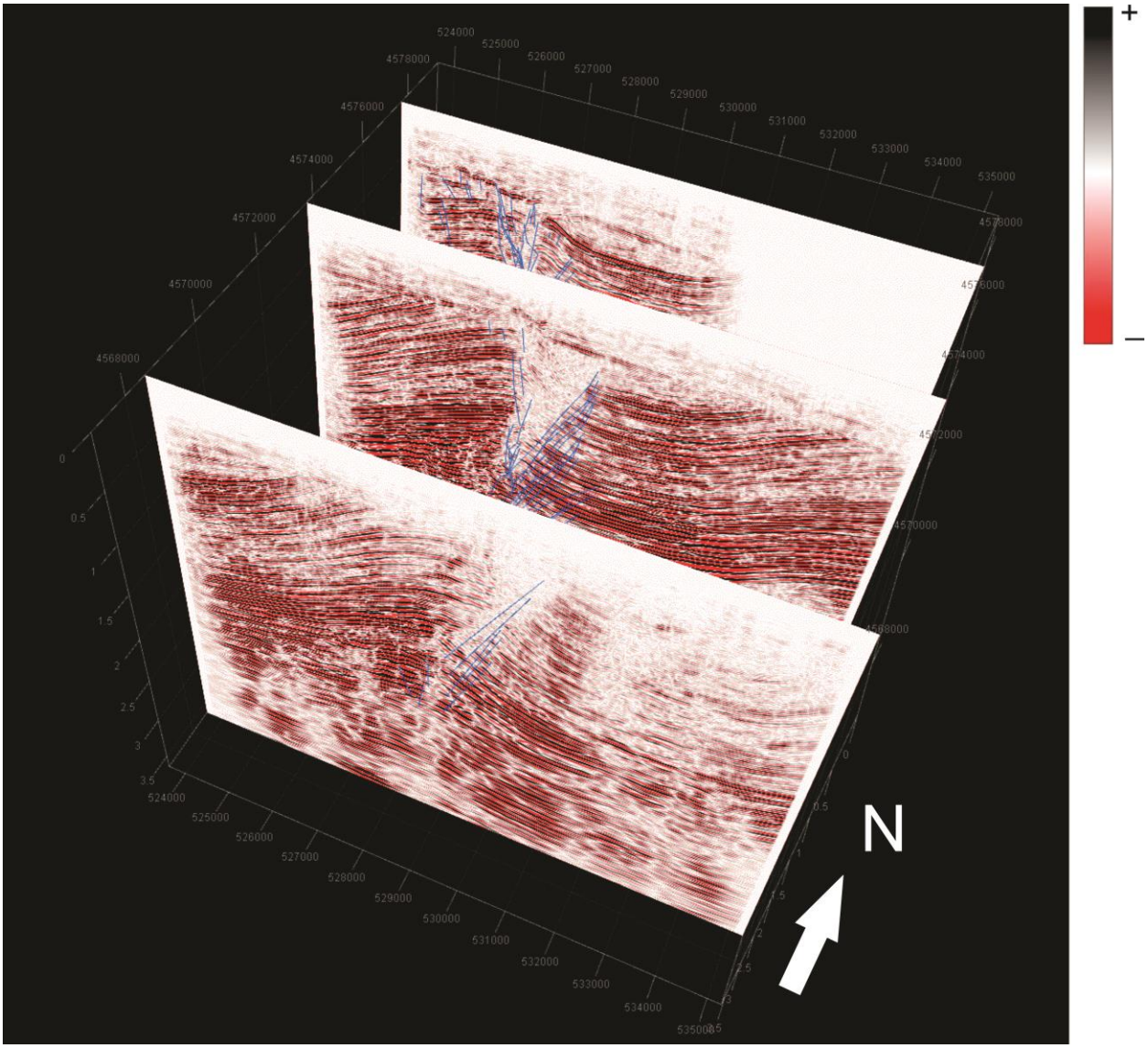

Figure 4.13: 3D perspective view of the study area (view from the south) showing the anticlinal fold and associated faults. The fold axis and the faults strike northwest-southeast and are truncated beneath the Miocene unconformity.

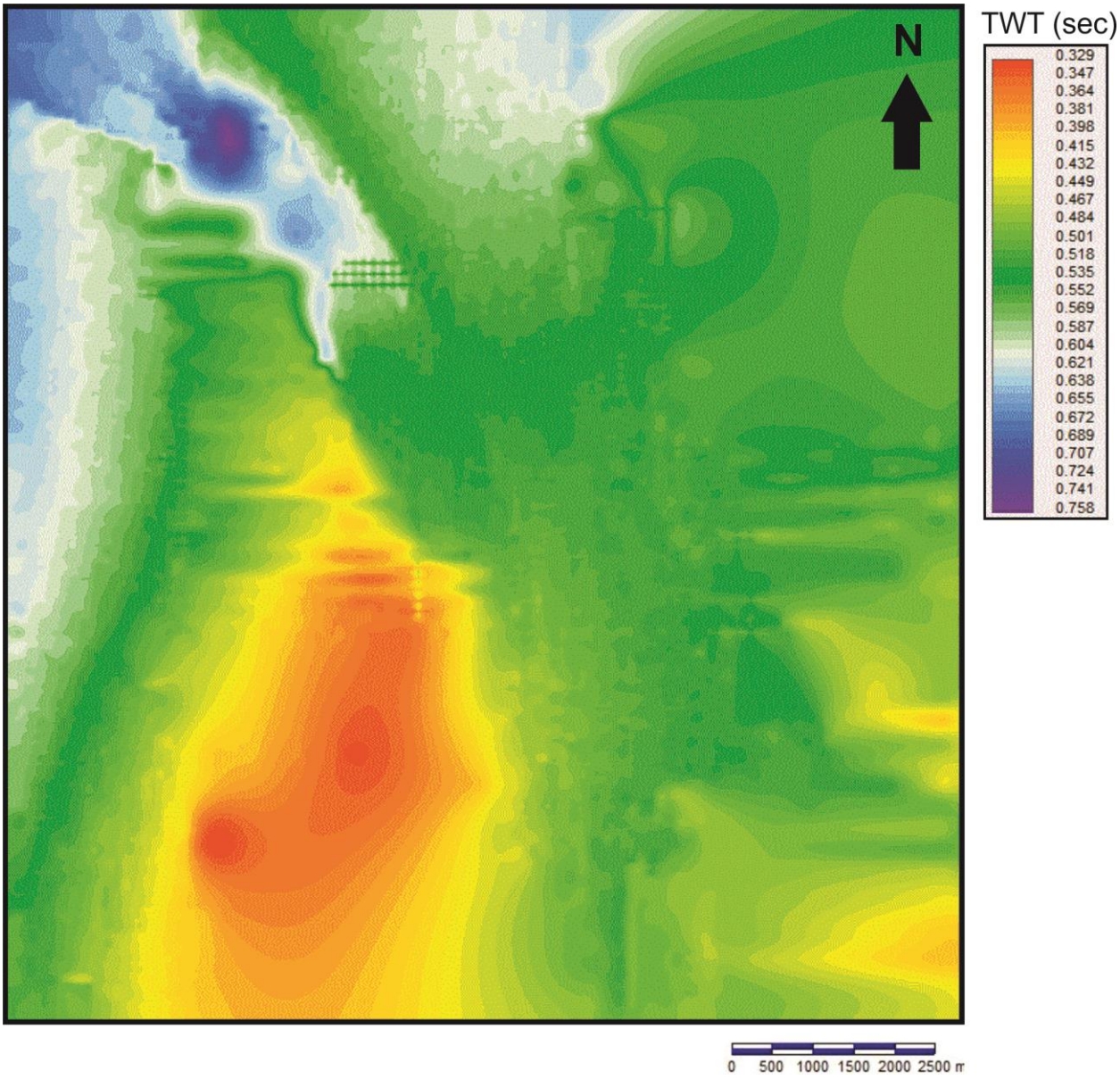

Figure 4.14: Time-structure contour map of the top of the Danismen Formation. Note that the formation top coincides with the angular unconformity and is mostly subhorizontal with shallowing over the anticlinal fold-fault system and local deepening in the northwest.

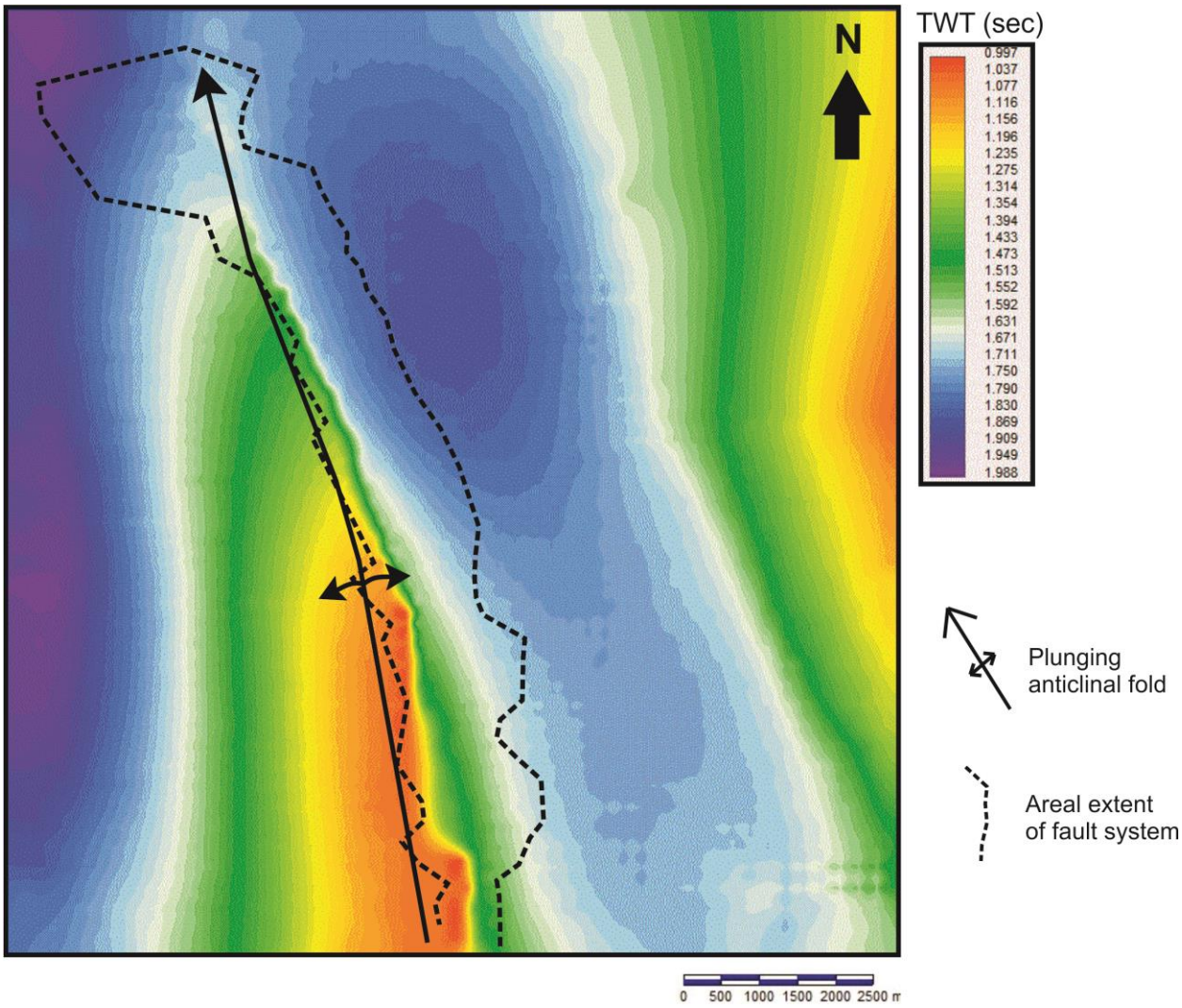

Figure 4.15: Time-structure contour map of top of the Osmancik Formation. Note that the formation top is shallowest above the anticlinal fold-fault system and in the east, and deepens to the east and west away from the central anticline.

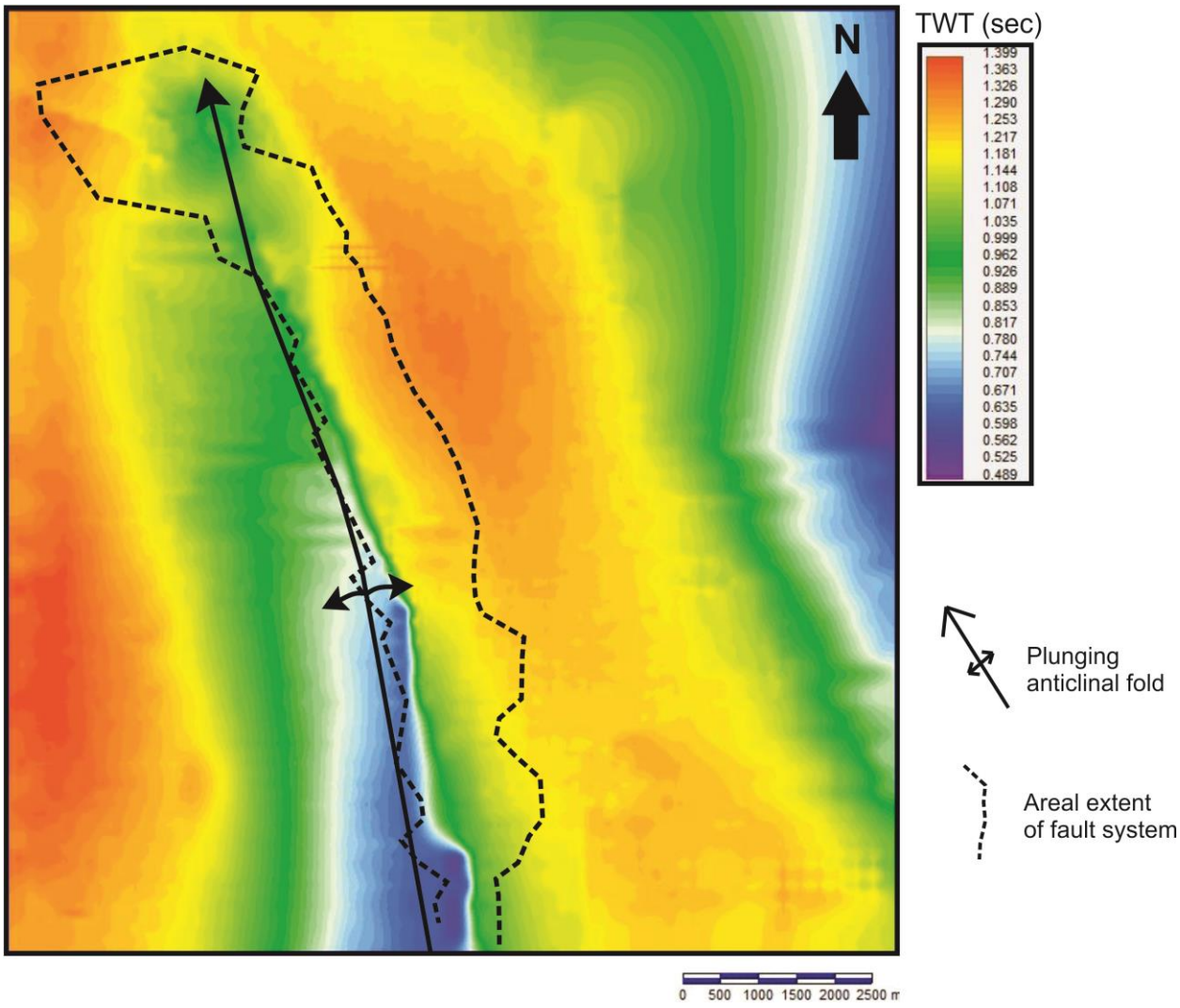

Figure 4.16: Isochron (thickness) map for the Danismen Formation showing thickness differences in a time domain. The Danismen Formation thins over the fold and in the east and thickens to the east and west of the fold trend.

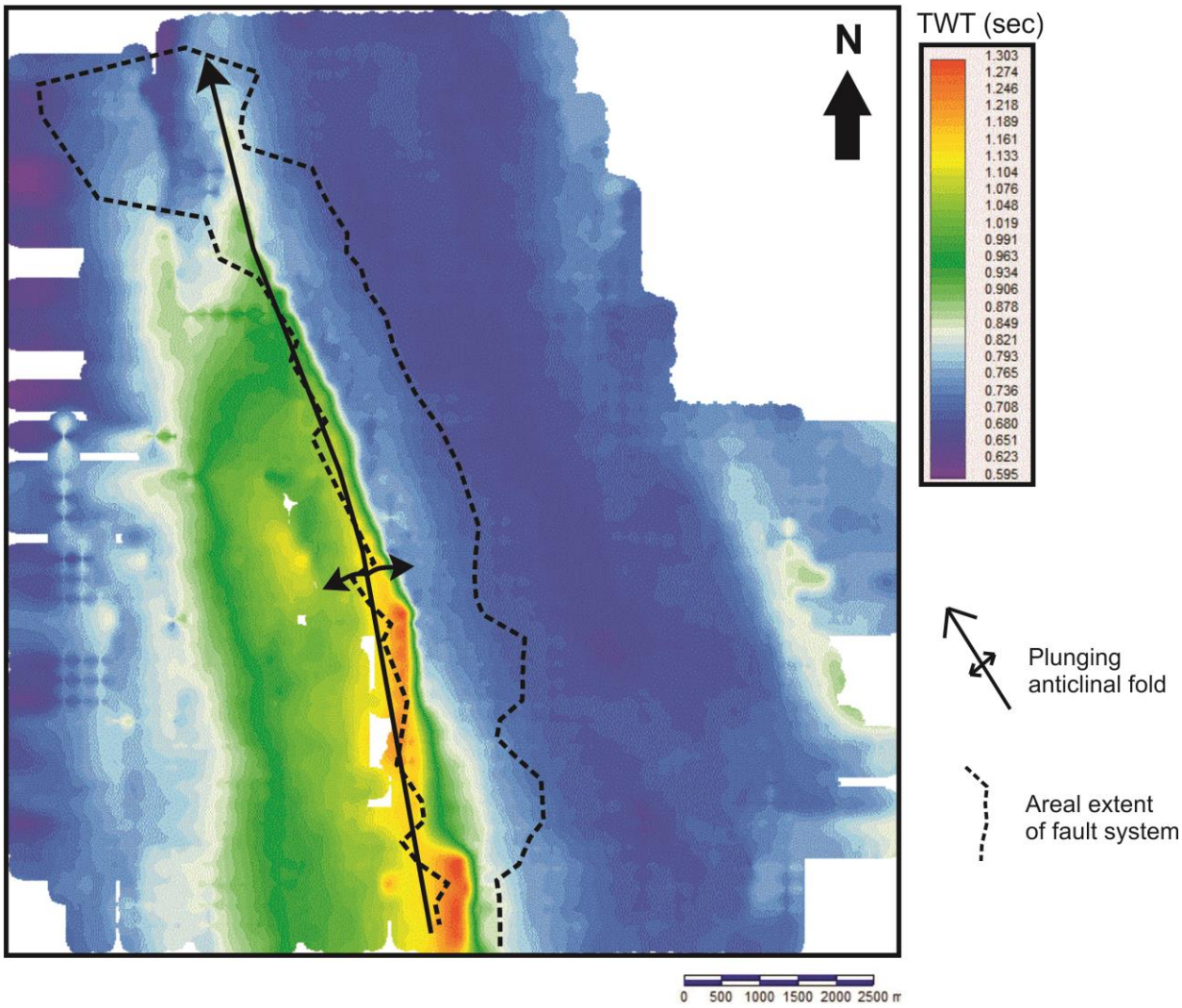

Figure 4.17: Isochron (thickness) map for the Osmancik Formation showing thickness differences in a time domain. The Osmancik Formation thickens over the anticlinal fold-fault system and thins to the east and west.

4.2. Well Log Analysis

Porosity has been determined using mainly density and neutron logs. Density-derived porosity (DPHI), neutron-derived porosity (NPHI), and total porosity (PHIT) have been calculated and are listed on the Table 4.1 for the target formations. Calculating density-derived porosity, some assumptions have been made. Matrix density is assumed to be 2.644 g/cm^3 and fluid density is assumed to be 1 g/cm^3. Furthermore, based on the Larionov's equation for shale volume calculation, shale-correction has been applied to the calculations and effective porosities have also been calculated. Table 4.2 displays the average values of shale-corrected density porosity (PHIDE), shale-corrected neutron porosity (PHINE), and total effective porosity (PHIE) for the target formations. Figures 4.18, 4.19 and 4.20 display porosity log curves for three wells and show the variations in porosity with depth. In general, porosity decreases with depth to around 1500 m in Well-1, to around 1100 m in Well-2 and for the full extent of Well 3. Below 1500 m in Well-1 and 1100 m in Well-2 porosity remains constant. However, it should be noted that drilling breaks are present in Well-1 (around 1400m) and Well-2 (around 1100m). In addition, whereas caliper logs are available for the three wells, bit size logs are only available for the Well-2. In Well-2 (Fig. 4.19), "cave-in" patterns through the upper part of the well indicate either brittle shaly intervals or "bad hole" conditions. High porosity spikes correlate with high caliper spikes but do not negate the general observation that porosity decreases with depth in the upper half to 2/3rds of the wells (Figs. 4.18, 4.19 and 4.20).

Table 4.1: Average of neutron, density and total porosity values.

Porosity (%)	Well 1			Well 2			Well 3		
	DPHI	NPHI	PHIT	DPHI	NPHI	PHIT	DPHI	NPHI	PHIT
Danismen	23	33	28	23	34	28	21	26	24
Osmancik	8	23	15	11	26	18	16	22	19

Table 4.2: Average of shale-corrected neutron, density and total porosity values.

Effective Porosity (%)	Well 1			Well 2			Well 3		
	PHIDE	PHINE	PHIE	PHIDE	PHINE	PHIE	PHIDE	PHINE	PHIE
Danismen	20	29	25	15	22	22	17	21	20
Osmancik	4	19	14	4	16	15	10	16	15

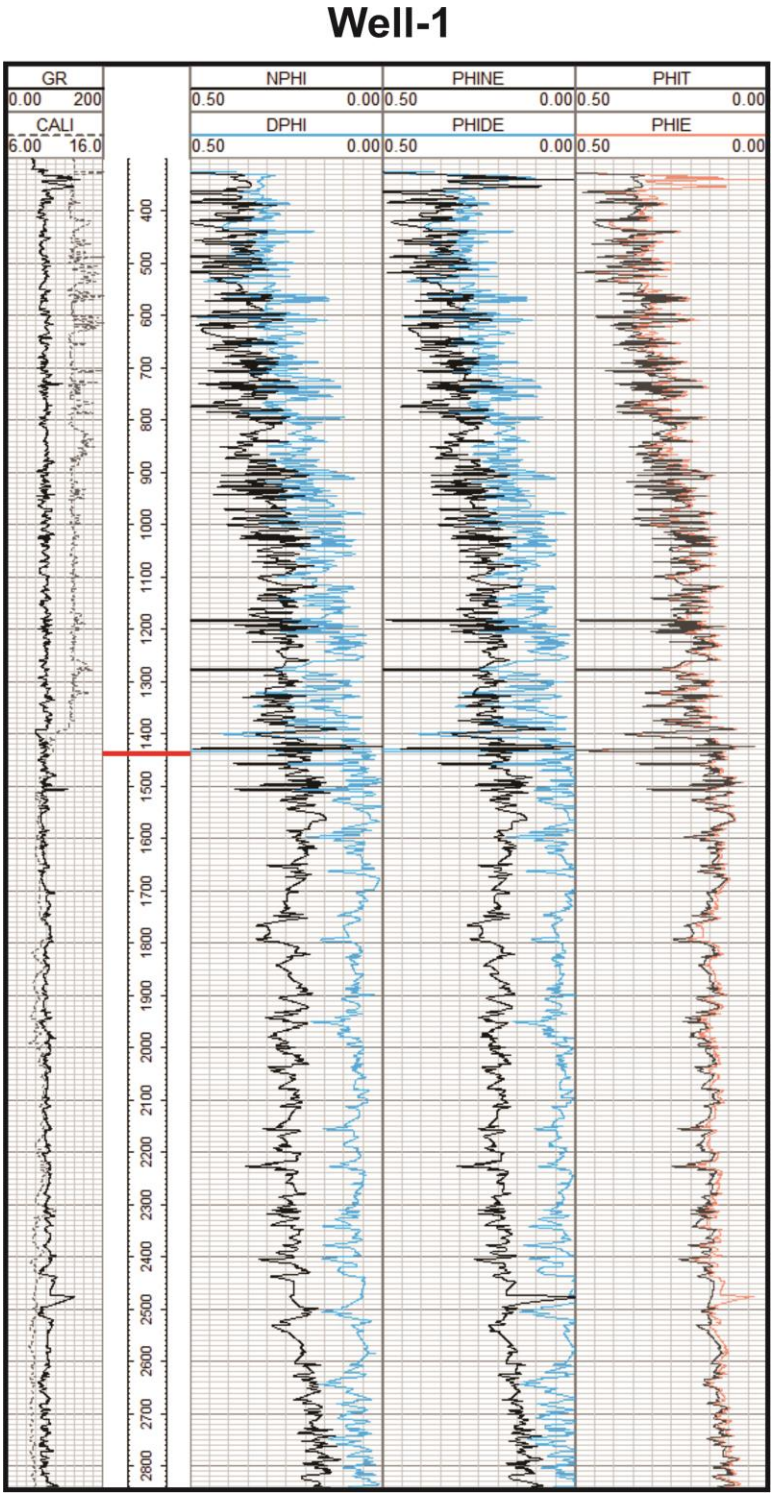

Figure 4.18: Porosity logs for Well 1. Top of Osmancik shown by red line. NPHI: Neutron-derived porosity, DPHI: Density-derived porosity, PHIDE: Shale-corrected density porosity, PHINE: Shale-corrected neutron porosity, PHIT: Average porosity, PHIE: Shale-corrected effective porosity. In general, porosity decreases with depth to around 1500 m and remains constant below this depth. Note drill break at about 1400 m.

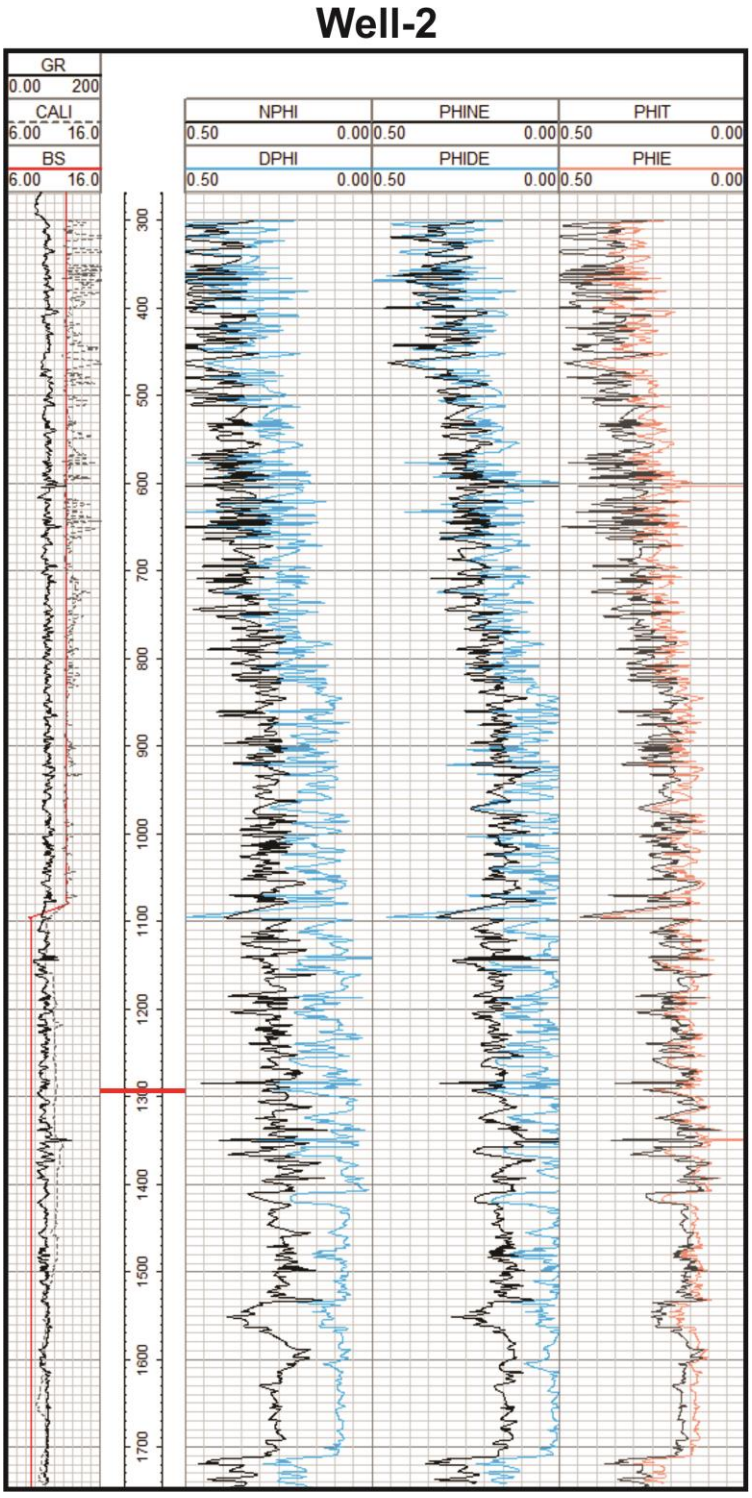

Figure 4.19: Porosity logs for Well 2. Top of Osmancik shown by red line.NPHI: Neutron-derived porosity, DPHI: Density-derived porosity, PHIDE: Shale-corrected density porosity, PHINE: Shale-corrected neutron porosity, PHIT: Average porosity, PHIE: Shale-corrected effective porosity. In general, porosity decreases with depth to around 1100 m and remains constant below this depth. Note drill break at about 1100 m.

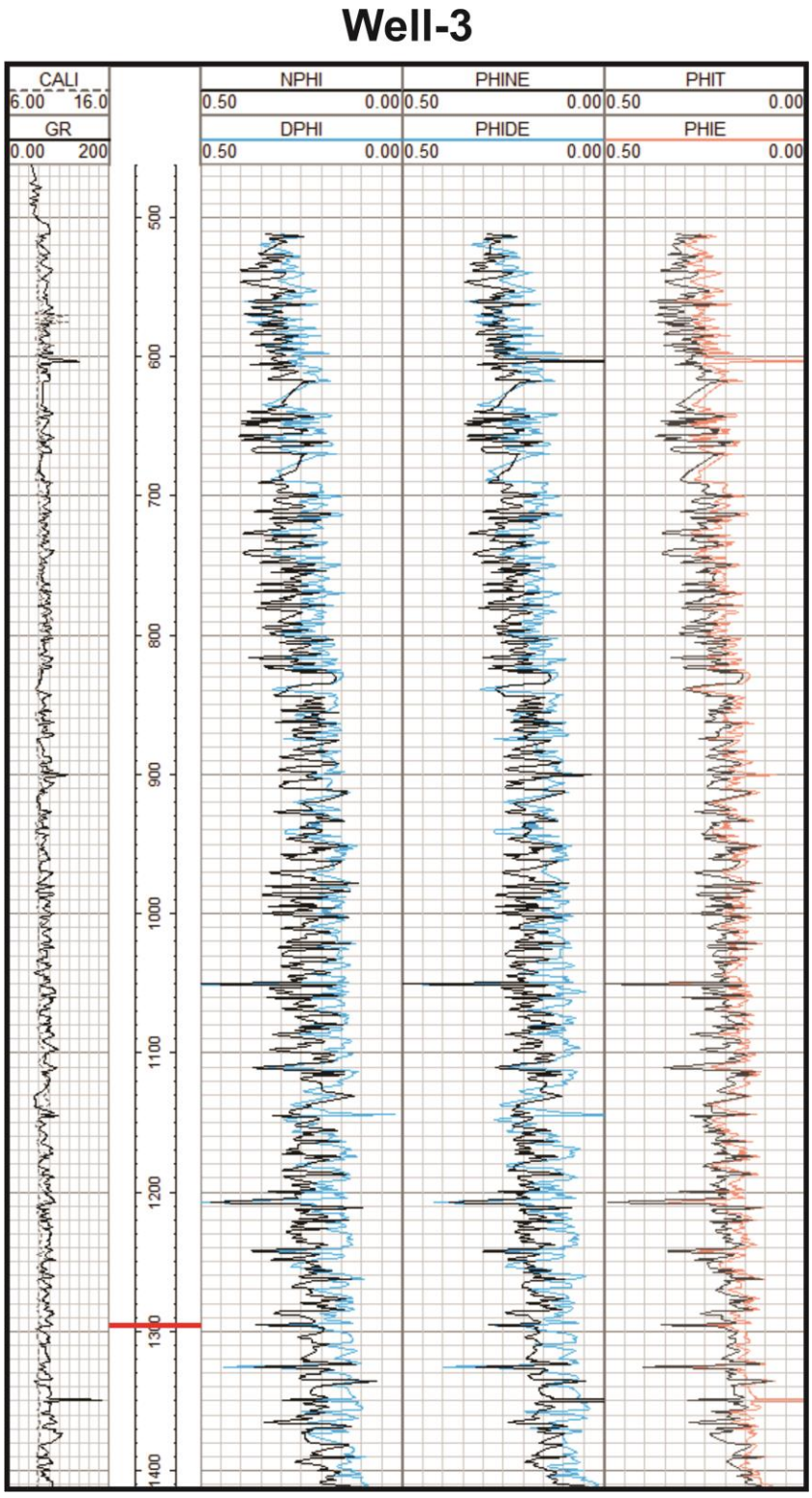

Figure 4.20: Porosity logs for Well 3. Top of Osmancik shown by red line. NPHI: Neutron-derived porosity, DPHI: Density-derived porosity, PHIDE: Shale-corrected density porosity, PHINE: Shale-corrected neutron porosity, PHIT: Average porosity, PHIE: Shale-corrected effective porosity. In general, porosity decreases progressively with depth.

To be able to differentiate clean sand zones from shaly-sand zones, volume of shale has to be calculated. In this study, shale volume was calculated based on GR logs. In particular, gamma ray index (IGR) has been calculated and a linear relationship of the GR log with shale volume have been generated. In Table 4.3, GR parameters for the equations are listed for the three wells. Additionally, non-linear equations have also been used to calculate shale volume in the strata. Hence, Larionov's (1969) shale volume equation for Tertiary rocks, Steiber's (1970) shale volume equation, and Clavier's (1971) shale volume equation have also been used to calculate the volume of shale. Figures 4.21, 4.22 and 4.23 illustrate shale volumes for the three wells and show the variation of shale volume with depth. Upper parts of the wells contain clean sands whereas the remainder of wells consists mainly of more shaly intervals with only local, thin sandstone intervals in the Osmancik Formation.

Table 4.3: Minimum and maximum GR readings from the logs for the shale volume parameters.

Vshale parameters	Well 1	Well 2	Well 3
GRmax	50	45	32
GRmin	150	125	130

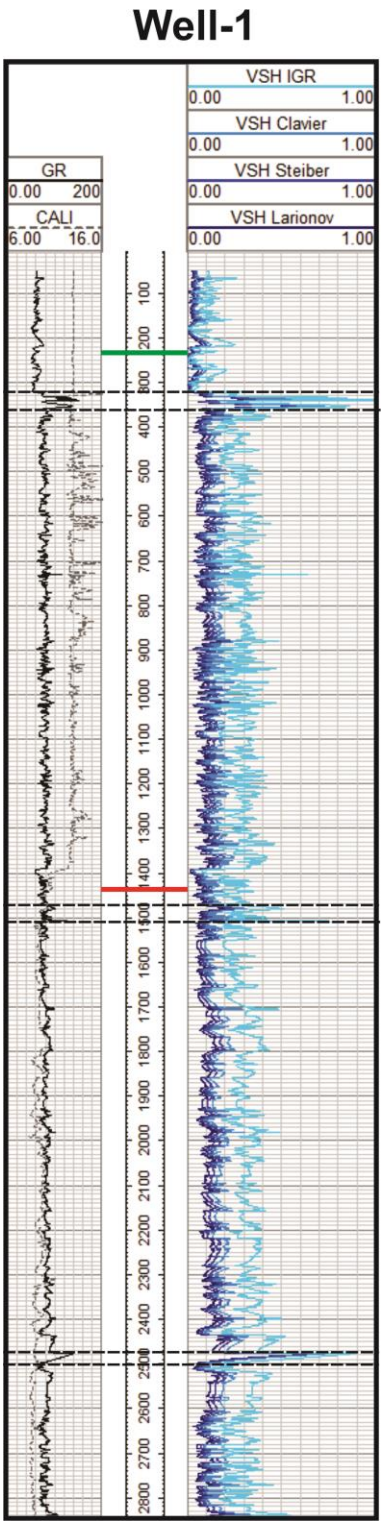

Figure 4.21: Well 1 showing shale volume changes down the borehole. Top of Osmancik shown by red line and top of Danismen shown by green line. Shale-rich intervals are shown with dashed lines. Shale volume of the formations changes 10-20 percent down the borehole.

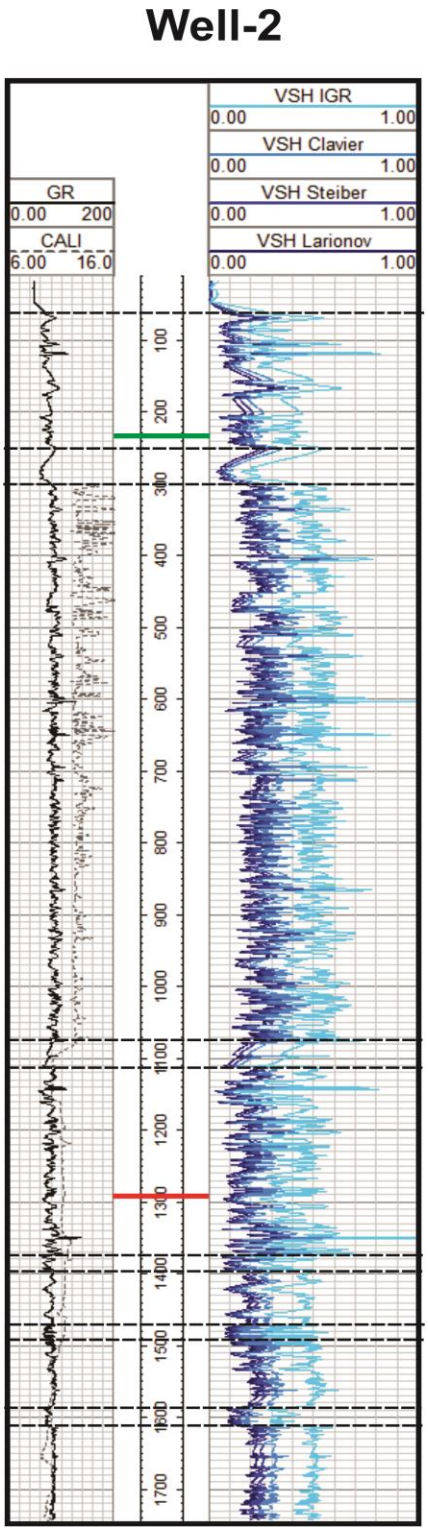

Figure 4.22: Well 2 showing shale volume changes down the borehole. Top of Osmancik shown by red line and top of Danismen shown by green line. Clean sand zones, marked with dashed lines, are developed mainly within upper Danismen Formation and locally within the Osmancik Formation.

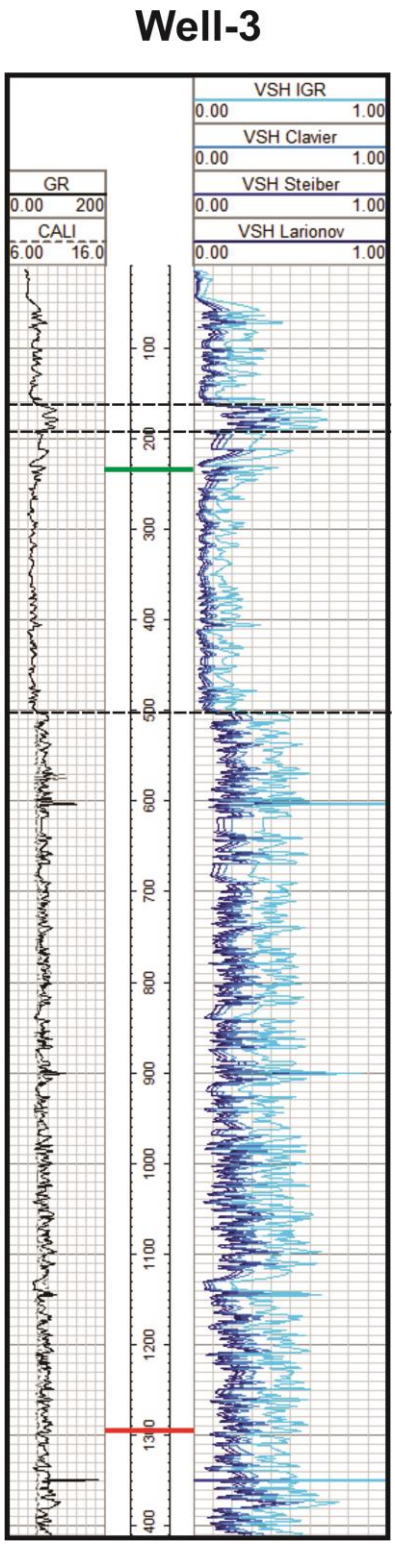

Figure 4.23: Well 3 showing shale volume changes down the borehole Top of Osmancik shown by red line and top of Danismen shown by green line. Dashed lines point the clean sand zones and shaly sand transitions. Clean sand zones are developed mainly within upper Danismen Formation and locally within the Osmancik Formation.

Water saturation is the ratio of water volume to pore volume. Thus, it is necessary to calculate water volume within pores to be able to understand the hydrocarbon content of reservoirs. Since water resistivity is not known, water saturation has been predicted using Pickett plots. Average porosity (PHIT) versus temperature-corrected deep resistivity (LLD @ Formation Temperature) has been used to interpret the saturation lines on the Pickett plot and is shown on the Figure 4.24, 4.25, and 4.26 for the three wells. Water resistivity values predicted from the plot are assumed to be %100 water-bearing zones. Accordingly, Table 4.4 shows water resistivity (Rw) value predictions from the Pickett plot. Moreover, calculated water saturation (Sw) and bulk volume water (BVW) values are displayed on Figure 4.27, 4.28, and 4.29 and illustrate changes in water saturation and BVW with depth. While saturation increases downward and to reach high highly water-saturation, BVW shows only a slight increase with depth due to the downward decrease in porosity.

Table 4.4: Water resistivity predicted values from the Pickett plot for the three wells.

	Well 1	**Well 2**	**Well 3**
Water Resistivity (Rw) (ohmm)	0.019	0.038	0.057

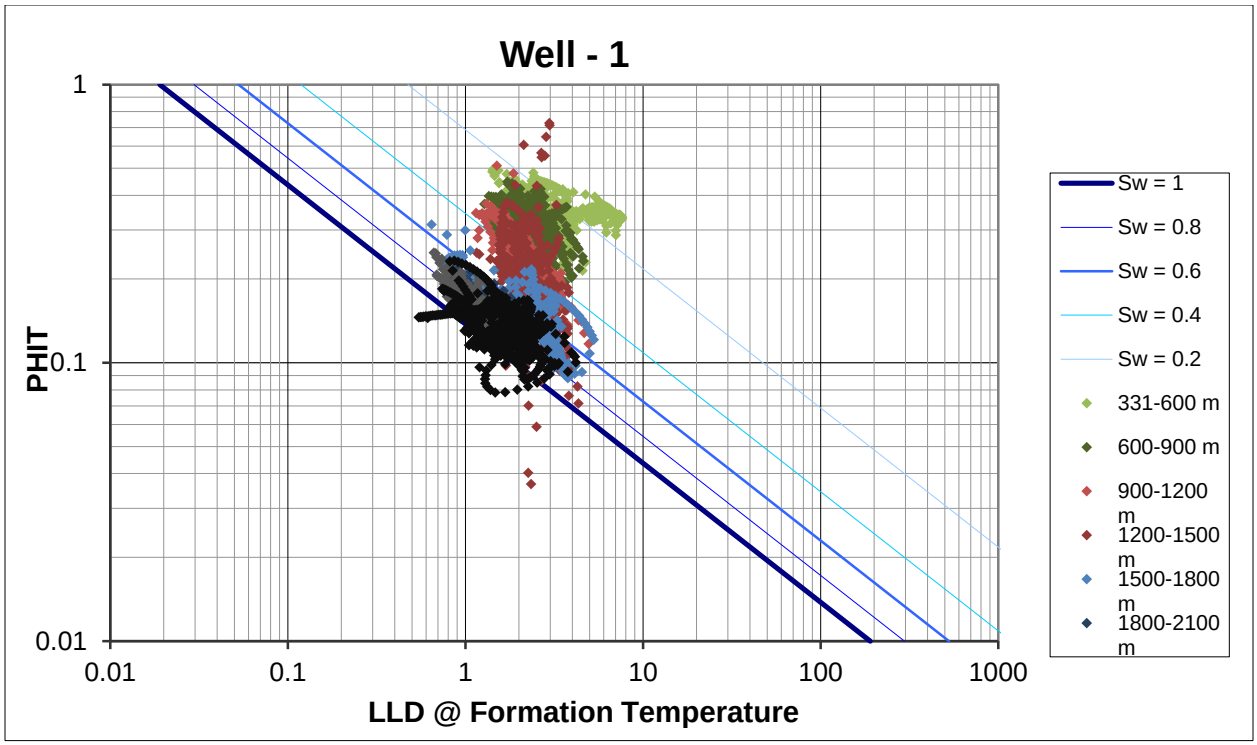

Figure 4.24: Pickett plot displaying average porosity (PHIT) versus resistivity (LLD) for Well 1. Water-bearing zones are identified and water saturations are calculated based on the prediction of Rw (water resistivity). Water-saturated zone is predicted from the arrangement of the data points and ranges up to 100% (1.0).

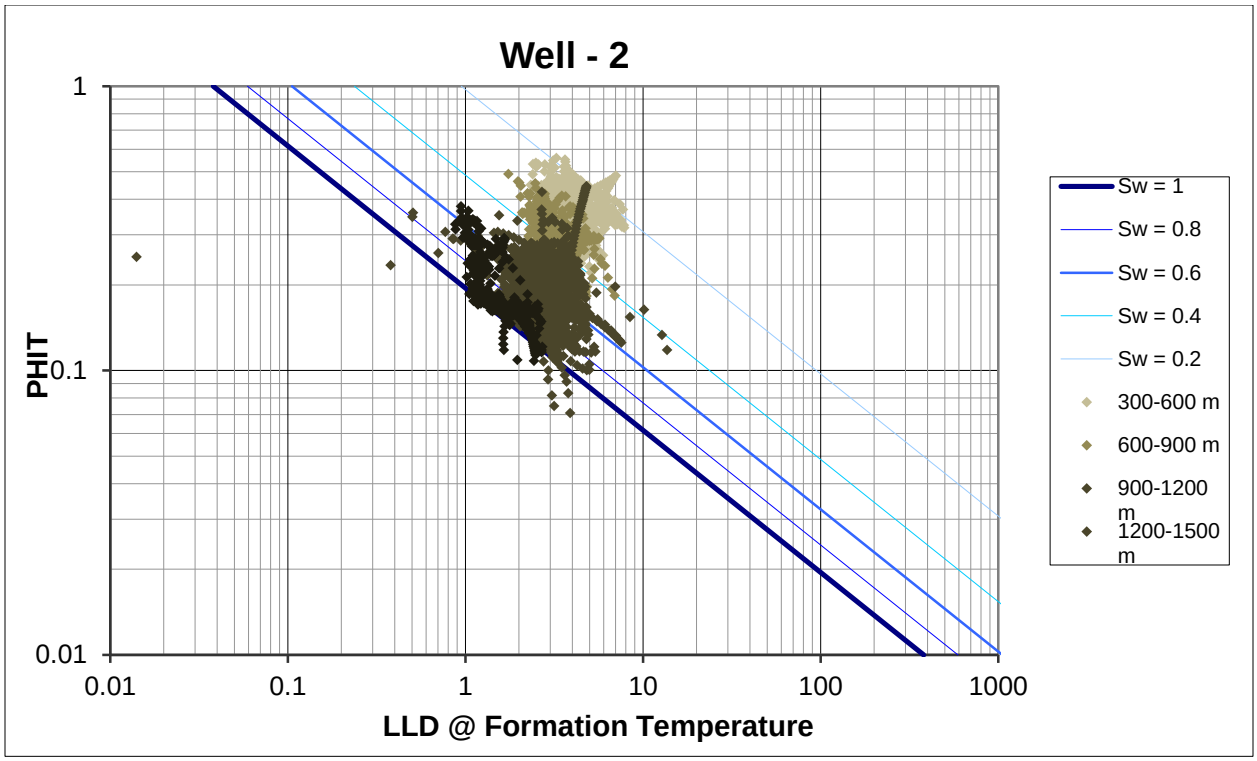

Figure 4.25: Pickett plot displaying average porosity (PHIT) versus resistivity (LLD) for Well 2. Water-bearing zone is identified and water saturations are calculated based on the prediction of Rw. Water-saturated zone is predicted from the arrangement of the data points and ranges up to 100% (1.0).

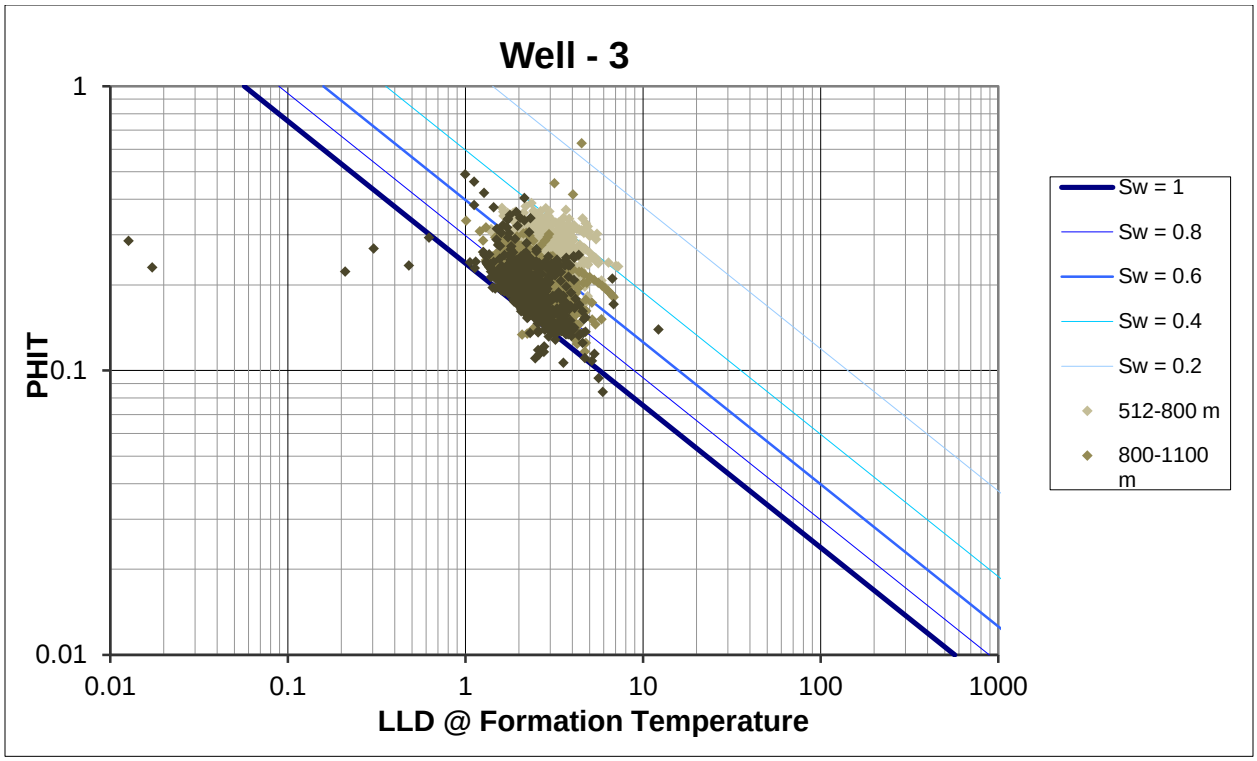

Figure 4.26: Pickett plot displaying average porosity versus resistivity for Well 3. Water-bearing zone is predicted and water saturations are calculated based on the prediction of Rw. Water-saturated zone is predicted from the arrangement of the data points and ranges up to 100% (1.0).

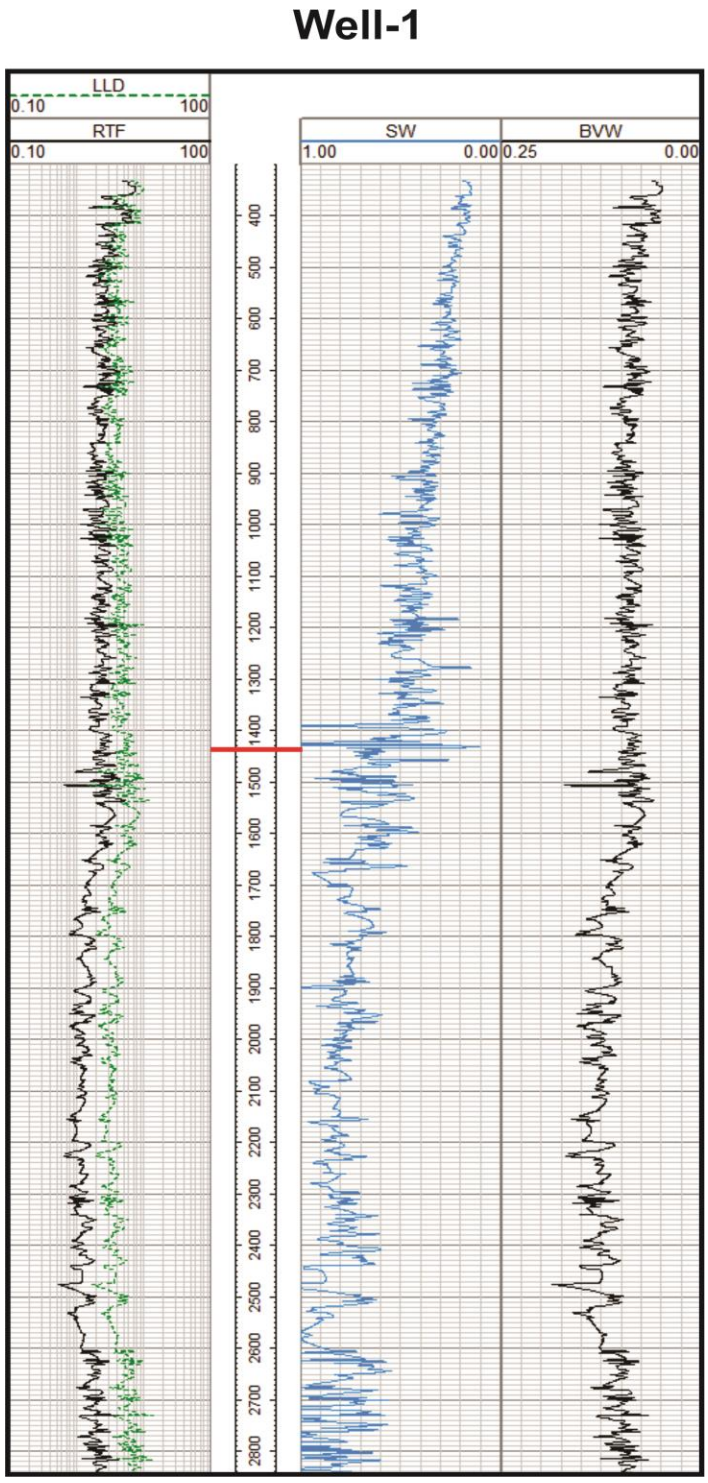

Figure 4.27: Water saturation (Sw) and Bulk Volume Water (BVW) for Well 1. Top of Osmancik shown by red line. In the first track, LLD and RTF (temperature corrected-LLD) are shown. In general, Sw increases with depth and reaches maximum water-saturation at depths of greater than 2400m. Local saturated zones are developed at shallower depths. BVW does not change quite as much since porosity decreases with depth.

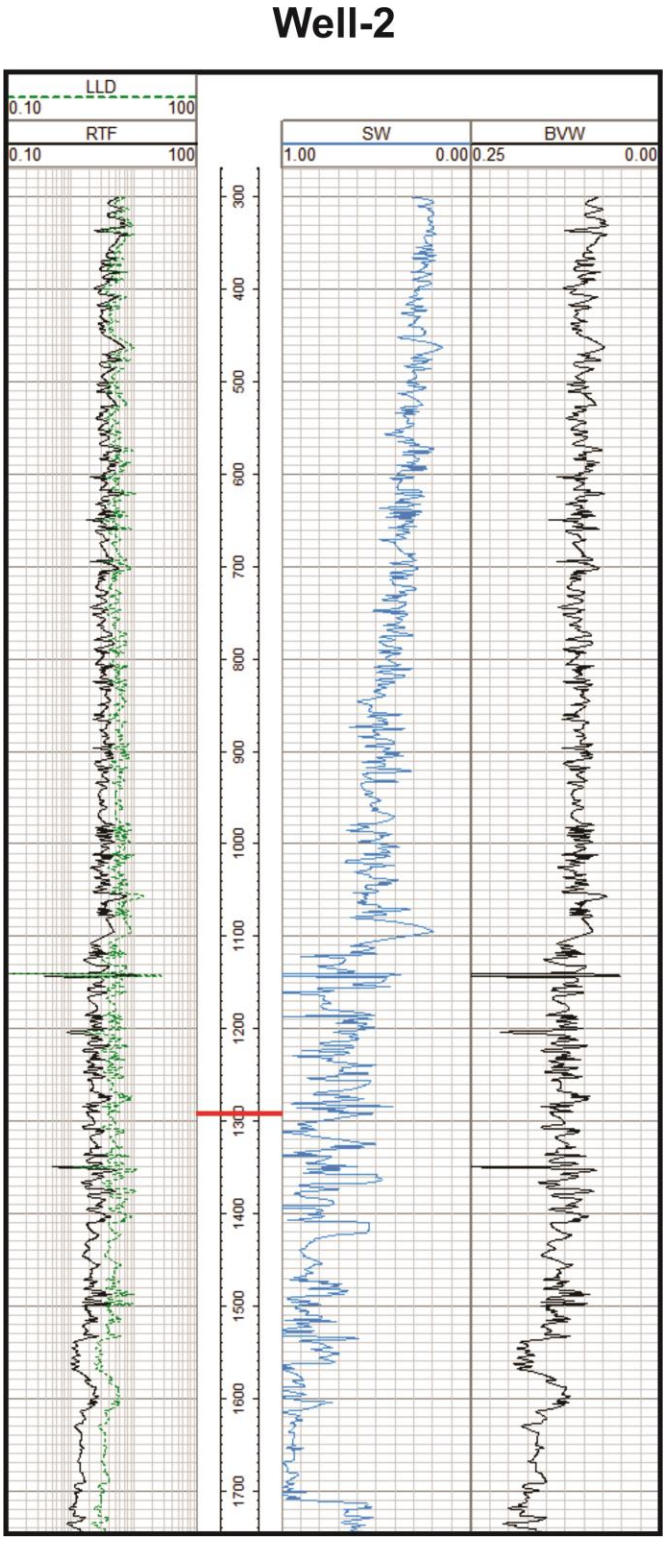

Figure 4.28: Water saturation (Sw) and Bulk Volume Water (BVW) for Well 2. Top of Osmancik shown by red line. In the first track, LLD and RTF (temperature corrected-LLD) are shown. In general, Sw increases with depth and reaches maximum water-saturation at depths of greater than 1100m. BVW does not change quite as much since porosity decreases with depth.

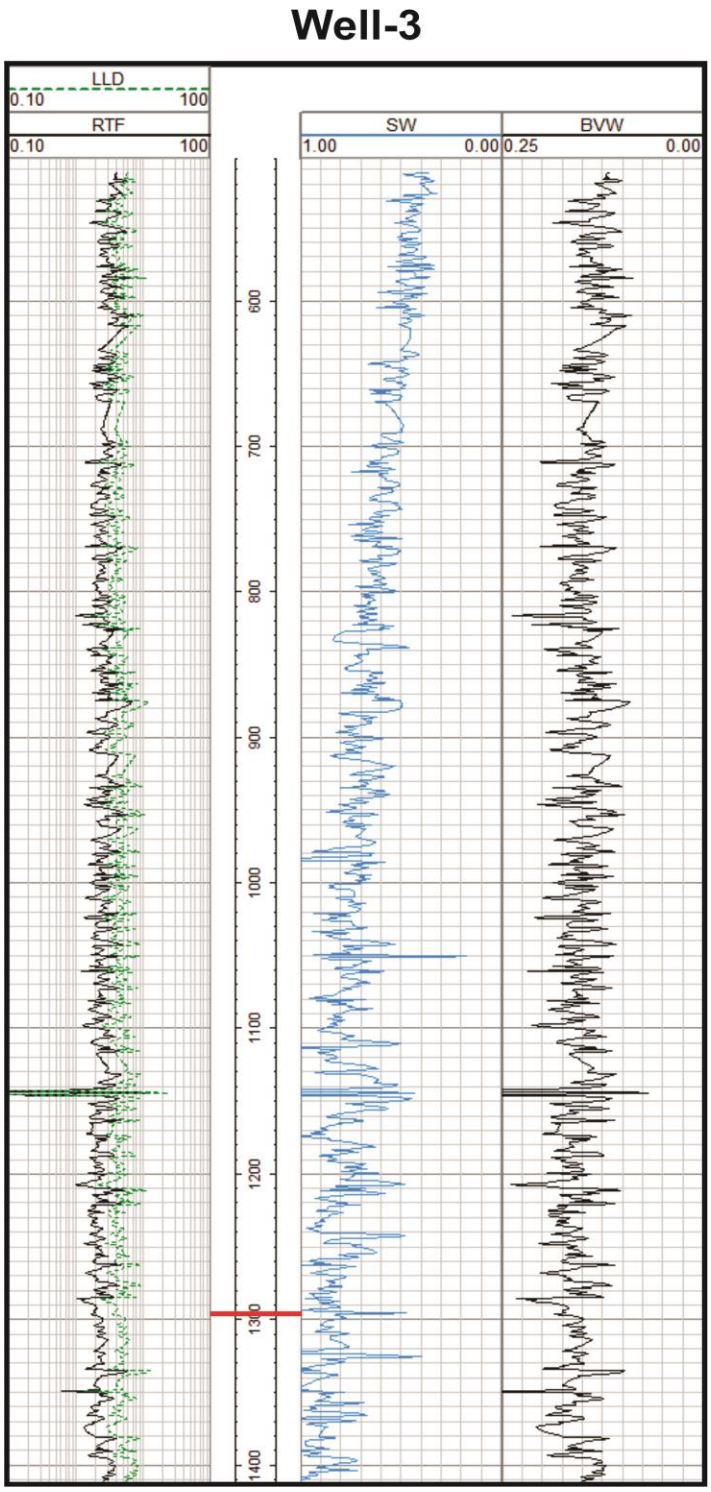

Figure 4.29: Water saturation (Sw) and Bulk Volume Water (BVW) for Well 3. Top of Osmancik shown by red line. In the first track, LLD and RTF (temperature corrected-LLD) are shown. In general, Sw increases with depth and reaches maximum water-saturation at depths of greater than 1300m. Local saturated zones are developed at shallower depths. BVW does not change quite as much since porosity decreases with depth.

Quick look methods can provide helpful insights to identify possible hydrocarbon zones. In this regard, apparent water resistivity (Rwa), wet resistivity (Ro), and Rxo/Rt ratio techniques have been taken into account to determine prominent zones which contains hydrocarbon. Figure 4.30, 4.31 and 4.32 display the relationships of these techniques for the three wells and show prominent hydrocarbon zones versus water zones. The resistivity ratio method (Rxo/Rt) is based on a comparison of resistivity ratio to SP logs. If the ratio is relatively constant and close to 1, shale is indicated. In water-bearing zones, the ratio tracks the SP curve, and in hydrocarbon-bearing zones, the ratio deflects from the SP curve (Asquith & Krygowski, 2004). In the apparent water resistivity (Rwa) method, lowest values of Rwa are most likely water saturated zones whereas greater Rwa values indicate hydrocarbon-bearing zones. Similarly, wet the resistivity (Ro) method indicates water or hydrocarbon saturated zones when it is compared with the deep resistivity. In this method, separation between the log curves is observed. If they overlay, this indicates a water-bearing zone. If they separate, this points to some hydrocarbon (Asquith & Krygowski, 2004). Hydrocarbon-bearing patterns are observed mainly in the upper parts of the wells whereas water-bearing zones are detected in the lower parts of the wells.

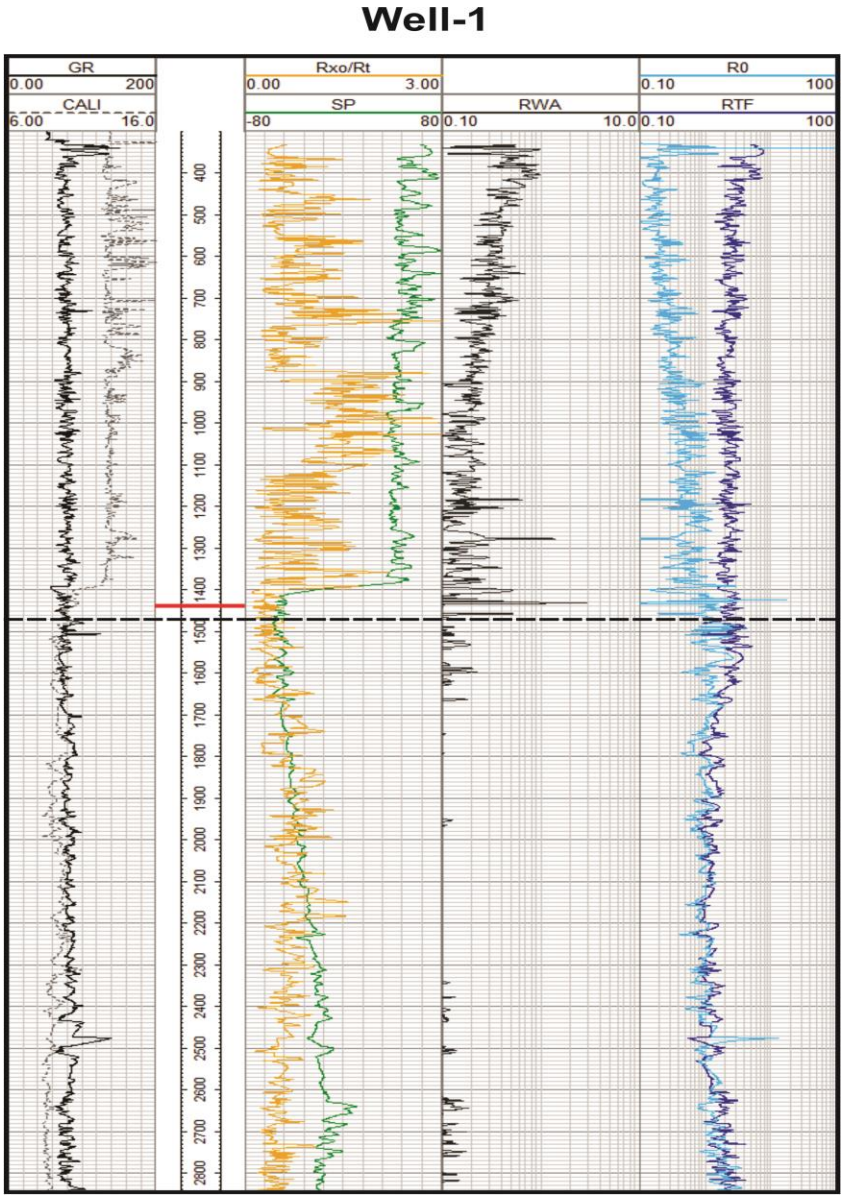

Figure 4.30: Quick look methods displaying Rxo/Rt ratio, apparent water resistivity (Rwa), and wet resistivity (Ro) for Well 1. Top of Osmancik shown by red line. Differentiation between hydrocarbons and water can be inferred from the patterns observed. In Tract 2: the comparison of the Rxo/Rt and SP log should display deflection from each other in hydrocarbon-rich zones and should track each other in water-rich zones. Rxo/Rt indicates shale when the ratio is close to 1. In Tract 3: Rwa values greater than true water resistivity values indicate the presence of hydrocarbons. Lower part of the well contains a water-saturated zone. In Track 4: The gap between the wet resistivity (Ro) and formation true resistivity (Rt) curves indicates hydrocarbon-bearing zones within the upper part of the well, and water zones where the gap closes and curves overlay in the lower part of the well. In general, the upper parts of the well contain hydrocarbon-bearing zones whereas lower parts of the well are mainly water-bearing. Dashed line divides the main hydrocarbon-bearing zone and water-bearing zone.

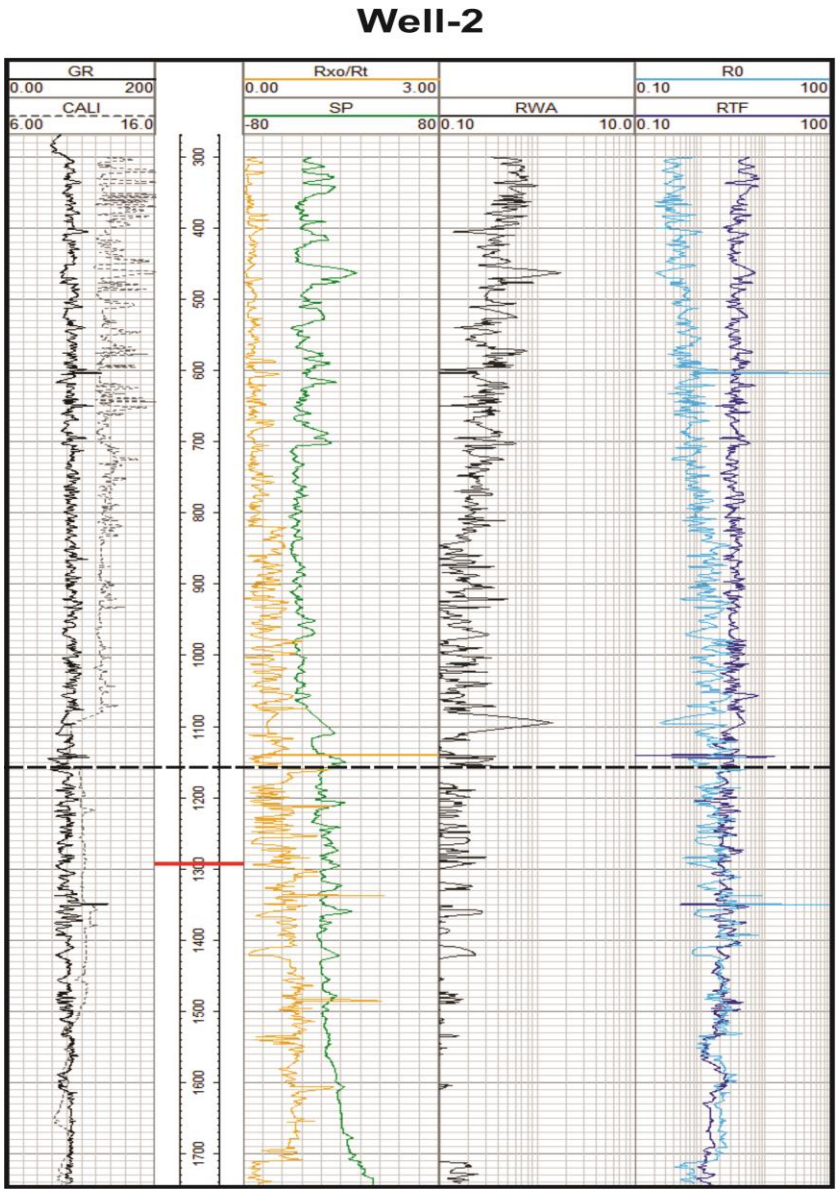

Figure 4.31: Quick look methods displaying Rxo/Rt ratio, apparent water resistivity (Rwa), and wet resistivity (Ro) for Well 2. Top of Osmancik shown by red line. Differentiation between hydrocarbons and water can be inferred from the patterns observed. In Tract 2: the comparison of the Rxo/Rt and SP log should display deflection from each other in hydrocarbon-rich zones and should track each other in water-rich zones. Rxo/Rt indicates shale when the ratio is close to 1. In Tract 3: Rwa values greater than true water resistivity values indicate the presence of hydrocarbons. Lower part of the well contains a water-saturated zone. In Track 4: The gap between the wet resistivity (Ro) and formation true resistivity (Rt) curves indicates hydrocarbon-bearing zones within the upper part of the well, and water zones where the gap closes and curves overlay in the lower part of the well. In general, the upper parts of the well contain hydrocarbon-bearing zones whereas lower parts of the well are mainly water-bearing. Dashed line divides the main hydrocarbon-bearing zone and water-bearing zone.

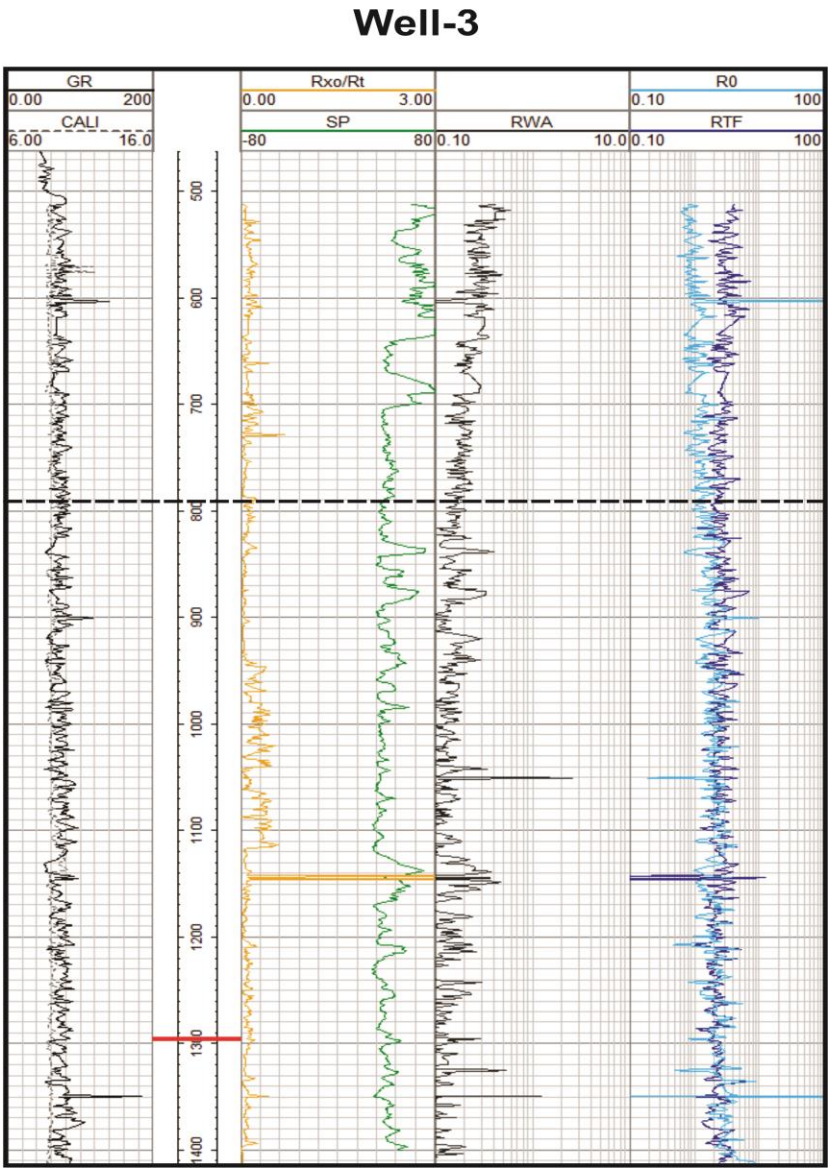

Figure 4.32: Quick look methods displaying Rxo/Rt ratio, apparent water resistivity (Rwa), and wet resistivity (Ro) for Well 3. Top of Osmancik shown by red line. Differentiation between hydrocarbons and water can be inferred from the patterns observed. In Tract 2: the comparison of the Rxo/Rt and SP log should display deflection from each other in hydrocarbon-rich zones and should track each other in water-rich zones. Rxo/Rt indicates shale when the ratio is close to 1. In Tract 3: Rwa values greater than true water resistivity values indicate the presence of hydrocarbons. Lower part of the well contains a water-saturated zone. In Track 4: The gap between the wet resistivity (Ro) and formation true resistivity (Rt) curves indicates hydrocarbon-bearing zones within the upper part of the well, and water zones where the gap closes and curves overlay in the lower part of the well. In general, the upper parts of the well contain hydrocarbon-bearing zones whereas lower parts of the well are mainly water-bearing. Dashed line divides the main hydrocarbon-bearing zone and water-bearing zone.

5. Discussion

5.1. Seismic Analysis Interpretation

The 3D seismic reflection survey permits differentiation of a number of seismic facies. The top of the Upper Oligocene, Danismen Formation coincides with the Miocene unconformity that is represented by a high-amplitude, continuous to semi-continuous, horizontal reflection around 0.4-0.5 seconds TWT (Figs. 4.6 - 4.9). This reflection also separates low-amplitude, parallel to semi-parallel and contorted, semi-continuous to discontinuous horizontal reflections above assumed to be the overlying Mio-Pliocene Ergene Group from high- to low-amplitude, continuous to semi-continuous, parallel, wavy reflections below representing the Danismen Formation. Seismic facies of the Danismen Formation consist of high- to low- amplitude, continuous to semi-continuous, parallel to semi-parallel reflections. Conversely, seismic facies of the Osmancik Formation consist of high- to moderate-amplitude, continuous to semi-continuous, parallel to semi-parallel, wavy reflections (Figs. 4.6 - 4.9). Beneath the Osmancik Formation, seismic facies are high- to low- amplitude, low frequency, semi-continuous to discontinuous, parallel to semi-parallel and horizontal reflections interpreted as the Mezardere Formation (Figs. 4.6 - 4.9). Table 5.1 summarizes the seismic facies identified within the seismic survey.

Additionally, a local fault system and a fold structure are identified within the seismic survey (Fig. 4.10 - 17). The fault structure is represented by low-amplitude, chaotic reflections throughout its extent and displays a positive flower structure on seismic sections. It is located within the target intervals, namely the Danismen and Osmancik formations and is most likely a right-lateral, strike slip fault associated with the basin inversion. The fold structure with a gentle, southwesterly limb and a steep, northeasterly limb is associated with the fault system and also developed during this transpressional regime. During Late Oligocene-Early Miocene period,

Thrace basin experienced a change in the regional stress field that resulted in a transition from transtension to transpression. As a result, Oligocene strata were uplifted and eroded along the Thrace-Eskisehir shear zone during Early Miocene. In Middle-Late Miocene, the Thrace-Eskisehir shear zone developed into a transpressional strike slip fault zone with associated folding (Sakinc et al., 1999). Alternatively, the local fold structure may be a fault propagation fold related to a reverse fault associated with NE-SW compression and that bottoms out in the lower Osmancik Formation or below as a layer-parallel fault. Evidence supporting this contention is the lack of deeply penetrating faults and the observation that whereas the northeastern limb of fold in the Osmancik and lower Danismen formation is faulted, in the Danismen Formation the fold is not offset but drapes over the fault system (Fig. 4.10). Both the fault system and the asymmetric fold are truncated beneath the Miocene unconformity and are thus dated as late Oligocene to early Miocene in age.

Deltaic deposits of the Danismen and Osmancik formations display a variety of seismic facies from which potential reservoir intervals can be identified. Two distinct seismic facies can be identified in the Danismen Formation that is made up mainly of sandstone and interbedded shale shale: (1) high-amplitude, continuous, parallel reflections that define clean sandstone intervals, and (2) moderate- to low- amplitude, semi-continuous, parallel to semi-parallel, and contorted reflections that are assumed to represent shaly intervals (Figs. 4.6 - 4.9). Similarly, two distinct seismic facies can be distinguished in the Osmancik Formation that consists of sandstone and subordinate shale: (1) high-amplitude, continuous, parallel reflections thought represent sandstone intervals, and (2) moderate- to low-amplitude, continuous to semi-continuous, parallel to semi-parallel reflections that probably represent shaly intervals (Figs. 4.6 - 4.9). On the basis of seismic data interpretation, the Danismen Formation has the highest content of prospective

reservoir rocks. The Miocene unconformity forms a stratigraphic trap across the survey area whereas the flower structure and associated fold constructs a northwest-southeast-trending structural trap across the extent of the study area.

Table 5.1: Seismic Facies Interpretation of the study area

Seismic Facies	Reflection Amplitude	Reflection Configuration	Reflection Continuity	Representative Image
Ergene Group	Low amplitude	Parallel to semi-parallel, contorted	Semi-continuous to discontinuous	
Danismen Fm	High amplitude	Parallel	Continuous	
	Moderate to low amplitude	Parallel to semi-parallel, contorted	Semi-continuous	
Osmancik Fm	High amplitude	Parallel	Continuous	
	Moderate to low amplitude	Parallel to semi-parallel	Continuous to semi-continuous	
Mezardere Fm?	High to low amplitude	Parallel to semi-parallel, contorted	Semi-continuous to discontinuous	

5.2. Well Log Analysis Interpretation

Potential reservoir zones identified on the seismic analysis are evaluated using well logs. Potential zones are characterized by higher resistivity with certain patterns (Rt>Ri>Rxo) indicating hydrocarbon concentrations. Cross-over of density and neutron porosity curves indicates occurrences of gas. Also interpreted from the well logs are clean sand intervals (shale volume less than 10%), low water saturation intervals, and correlation of effective porosity and bulk volume water showing water versus hydrocarbon concentration within pores (Table 5.2). Analysis of the well logs based on the above criteria reveals that the most promising zones are

present within Well 2 (Figs. 5.1, 5.2, and 5.3). Zonal distribution of potential reservoir intervals are also correlated with the GR logs between the wells. Five main reservoir intervals are defined and only one of them extends through Well 1 (Figs. 5.1, 5.2, and 5.3). Zone 1 in the Danismen Formation is the deepest reservoir interval and is observed in all wells. The thickness of this interval varies from 20 to 30 meters between the wells. Zone 1 is at around 1100 meters depth in Well 2, 1150 meters in Well 3 and deepens to around 1400m in Well 1. This zone trends parallel to the southwesterly dipping limb of the fold structure. Zone 2 in the Danismen Formation is identified only within Well 2 and Well 3 and is located at around 680 meters depth in Well 2 and 910 meters depth in Well 3. This zone similarly tracks the southwesterly dipping limb of the fold structure. The thickness of this interval varies from 20 to 30 meters. Zones 3 and 4 are located within the Danismen Formation, occur between 450-550 meters depth in Well 2 and 600-700 meters depth in Well 3 and have thicknesses of approximately 20 meters each. Zone 5 is the shallowest zone represented by a clean sand interval in the uppermost part of the Danismen Formation; only GR logs are available for this interval.

Table 5.2: Table showing prospective reservoir criteria

Zone Definition Criteria	Zone 1	Zone 2	Zone 3	Zone 4	Zone 5
Resistivity Pattern (Rt>Ri>Rxo)	✓	✓	✓	✓	-
Porosity Crossover indicating gas presence	✓	✓	✓	✓	-
Clean Sandstone Intervals (shale volume less than 10%)	✓	✓	✓	✓	✓
Relatively Decreasing Water Saturation	✓	✓	✓	✓	-
Effective porosity vs BVW represented with a high spike indicating hydrocarbon concentration	✓	✓	✓	✓	-

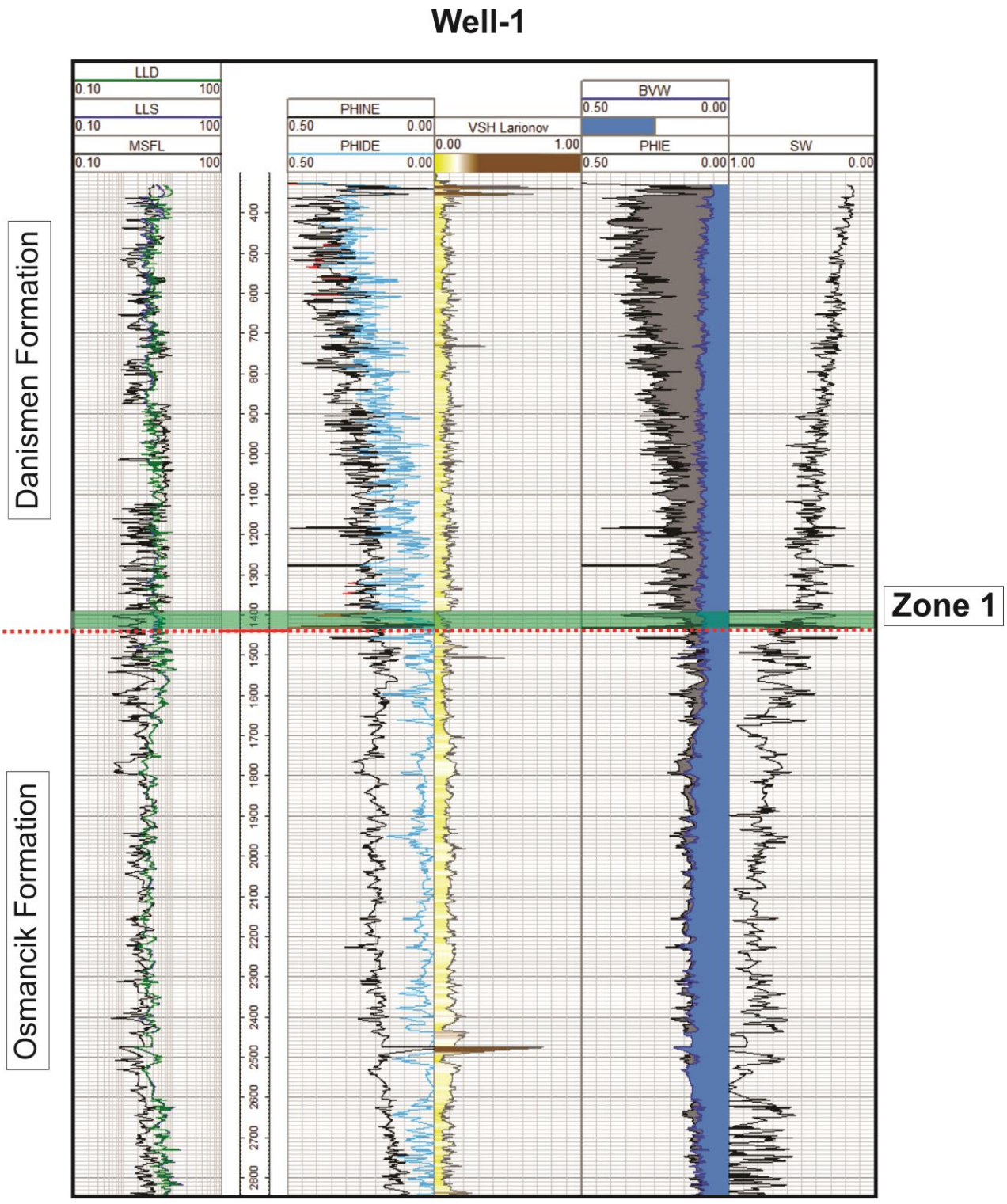

Figure 5.1: Evaluation of the Well Log 1 showing prominent reservoir zones. This well contains one prospective reservoir zone in the Danismen Formation. Note that the reservoir zones display clean sand intervals with low water saturation, relatively higher resistivity, and porosity crossover indicating gas.

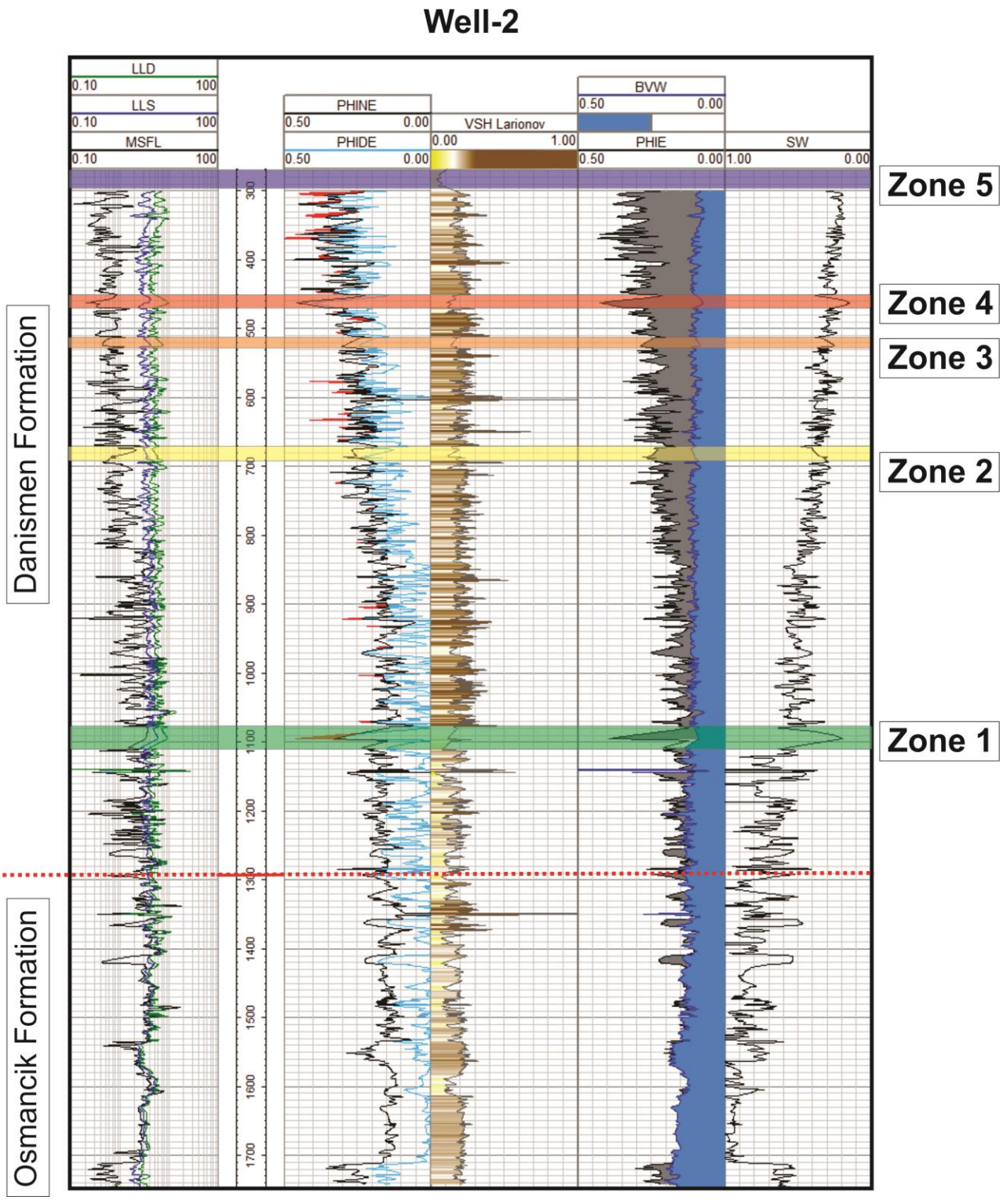

Figure 5.2: Evaluation of the Well Log 2 showing prominent reservoir zones. This well contains five prospective reservoir zones in the Danismen Formation. Note that reservoir zones display clean sand intervals with low water saturation, relatively higher resistivity, and porosity crossover indicating gas.

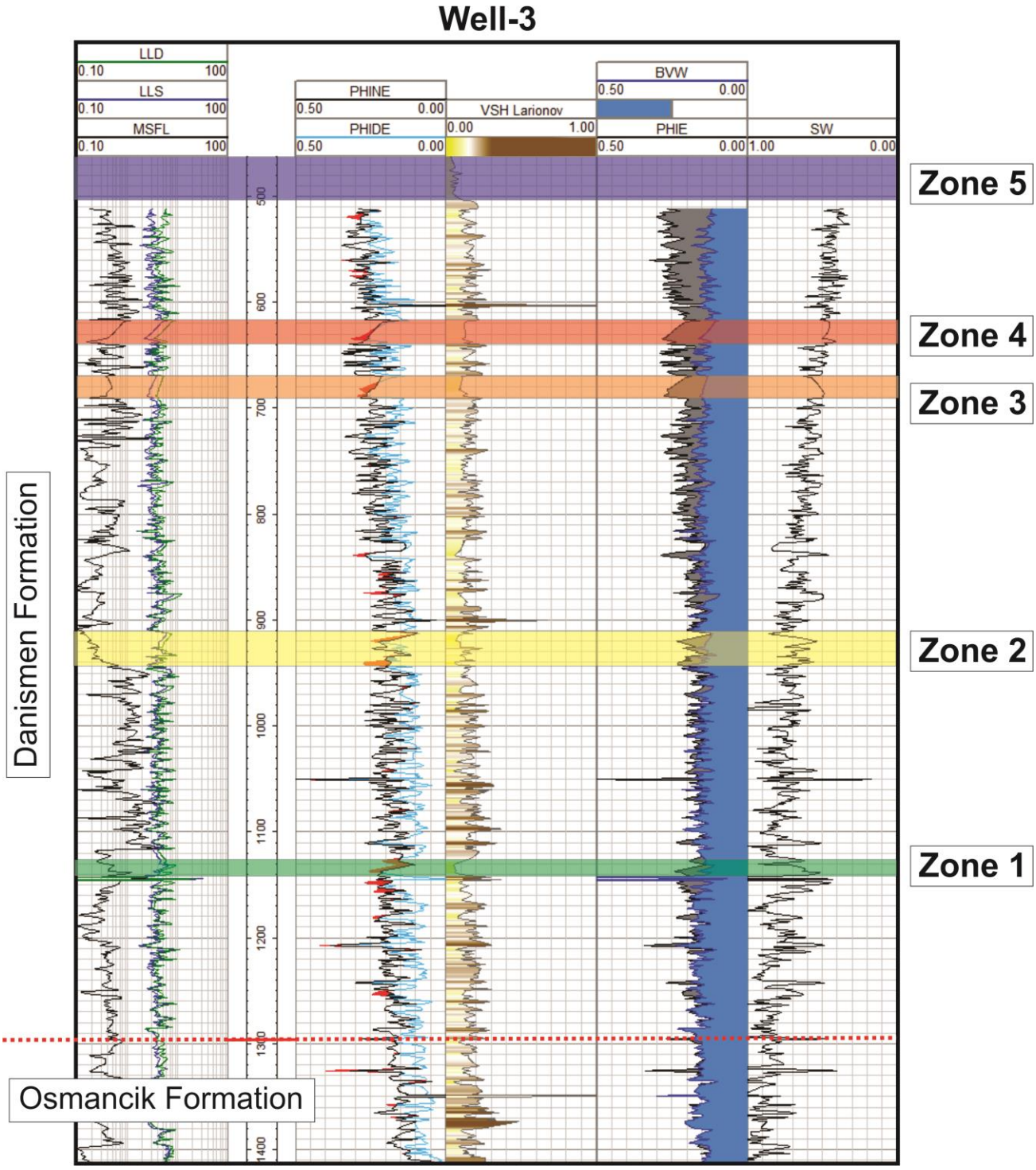

Figure 5.3: Evaluation of the Well Log 3 analysis showing prominent reservoir zones. This well contains five prospective reservoir zones in the Danismen Formation. Note that reservoir zones display clean sand intervals with low water saturation, relatively higher resistivity, and porosity crossover indicating gas.

5.3. Integration of Seismic and Well Log Analysis

The depth trend of the five zones identified in this study follows the trend of the southwesterly dipping limb of the fold structure. Hydrocarbon concentrations increase through the fold structure in the study area. Identified zones represent hydrocarbon-bearing, clean sand intervals and should specifically be evaluated as potential target reservoirs. Clean sandstones in the upper part of the Danismen Formation have the highest prospectivity as hydrocarbon reservoirs. This analysis has demonstrated that the fault system and associated asymmetric fold was the main factor that affected the zonal distribution of hydrocarbons across the study area (Fig 5.4). Therefore, target intervals should be tracked throughout the areal extent of the fold structure. Besides, although logs are not available for the uppermost part of the Danismen Formation (Zone 5), it is highly recommended that this wedge-shaped zone (Fig. 5.4) be evaluated as a good reservoir with relatively thick clean sand confined by the fold structure and the unconformity. Moreover, Well 2 exhibits hydrocarbons concentrated in alternating sandstone and shale within the upper half of the Danismen Formation that also warrant evaluation as prospective reservoirs.

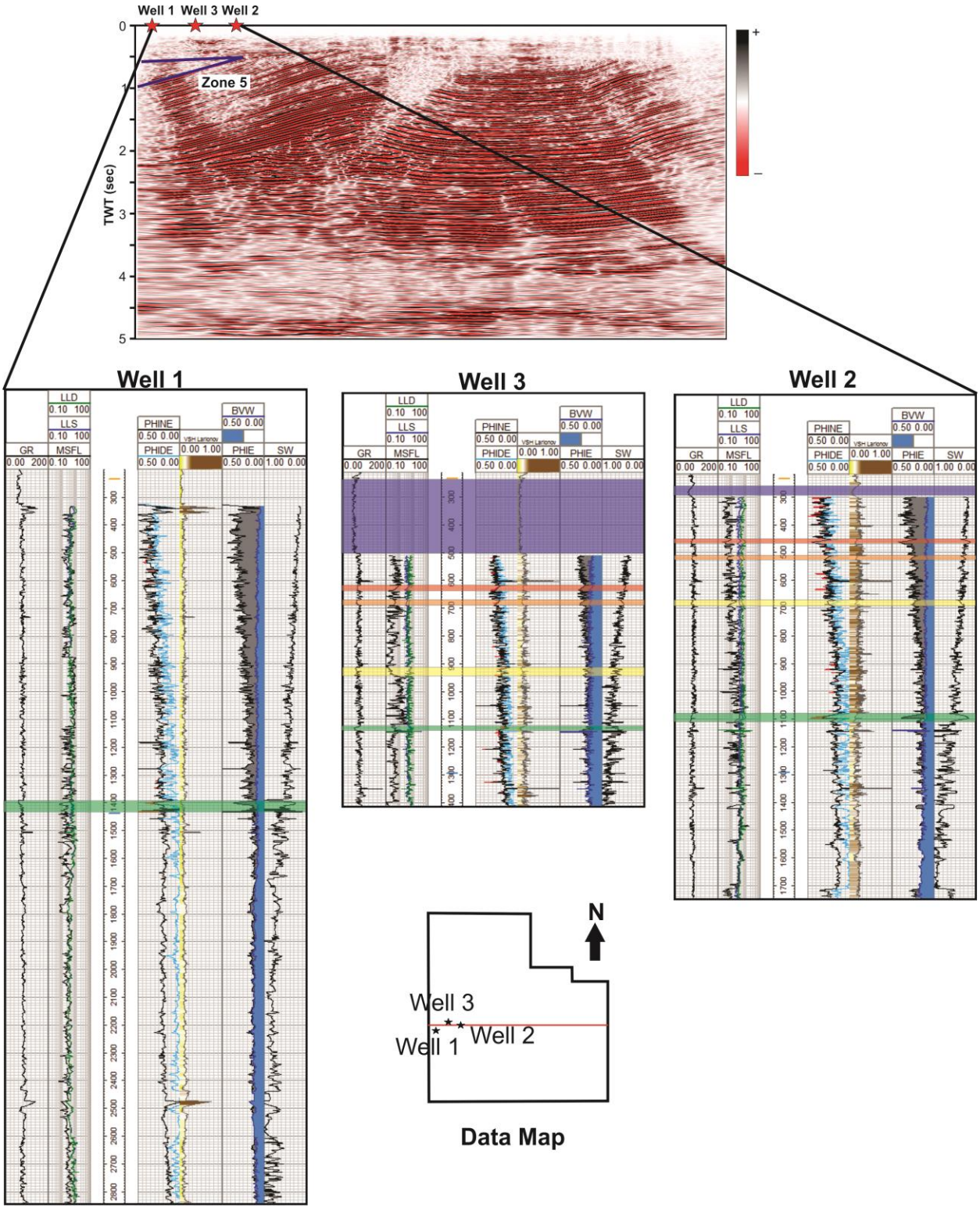

Figure 5.4: Cross-section displays the correlation of the potential reservoir distribution in the study area. Hydrocarbon concentration increases through the fold structure and fault system as seen in the seismic image. Zone 5 is marked on the seismic cross-section.

6. Conclusions

This research investigated prospective reservoirs in Oligocene deltaic sandstones in the Thrace Basin utilizing 3D seismic reflection survey (covering approximately 120 km^2) and wireline logs from three wells. The geometric configuration of strata in the study area was delineated and target formations identified using 3D seismic reflection data. A NW-SE trending fold structure and a local fault system, interpreted as a right-lateral strike slip fault or reverse fault, were mapped across the study area. Both the fault system and the asymmetric fold are truncated beneath the Miocene unconformity and are thus dated as late Oligocene to early Miocene in age.

Petro-physical properties of the Oligocene Danismen and Osmancik formations were determined using wireline logs to evaluate potential target reservoirs. Five main zones representing hydrocarbon-bearing clean sandstone intervals have the highest prospectivity as potential reservoirs. Although logs are not available for the uppermost Danismen Formation, Zone 5 is identified as a good reservoir with relatively thick clean sand confined by the unconformity and the fold structure. The depth trend of these five prospective zones follows the depth trend of the southwesterly dipping limb of the fold structure. Hydrocarbon concentrations increase through the fold structure. The fault system and associated asymmetric fold were the main factors that affected the zonal distribution of the hydrocarbons across the study area. The Miocene unconformity and the fault construct good trap settings for the hydrocarbons. Therefore, these potential zones should be tracked across the fold structure in order to determine the areal extent of the potential reservoirs within the study area.

REFERENCES

Alisan, C. (1985). Trakya “I” Bölgesi’nde Umurca-1, Kaynarca-1, Delen-1 kuyularında kesilen formasyonların palinostratigrafisi ve çökelme ortamlarının değerlendirilmesi. TPAO. Araştırma Grubu Rapor No:386. p. 60. Ankara (unpublished).

Archie, G. E. (1942). The electrical resistivity log as an aid in determining some reservoir characteristics. Journal of Petroleum Technology, v. 5, p. 54–62.

Asquith, G., & Krygowski, D. (2004). Basic well log analysis (second edition). The American Association of Petroleum Geologists. Tulsa, Oklahoma.

Bati, Z., Alisan, C., Ediger, V., Teymur, S., Akca, N., Sancay, H., Ertug, K., Kirici, S., Erenler, M., & Akoz, O. (2002). Kuzey Trakya Havzası’nın Palinomorf, Foraminifer ve Nannoplankton Biyostratigrafisi. Turkiye Stratigrafi Komitesi Calistayi (Trakya Bolgesi’nin Litostratigrafi Adlamalari) Ozleri (p. 14).

Bati, Z., Erk, S., & Akca, N. (1993). Trakya havzası Tersiyer Birimleri'nin Palinomorf, Foraminifer ve Nannoplankton Biyostratigrafisi. TPAO Araştırma Grubu Rapor No:1947. Ankara (unpublished).

Clavier, C., Hoyle, W., & Meunier, D. (1971). Quantitative interpretation of thermal neutron decay time logs: Part I. Fundamentals and techniques. Journal of Petroleum Technology, v. 23, p. 743–755.

Coskun, B. (2000). Influence of the Istranca-Rhodope Massifs and strands of the North Anatolian Fault on oil potential of Thrace Basin, NW Turkey. Journal of Petroleum Science and Engineering, v. 27(1–2), p. 1–25.

Dewan, J. (1983). Essentials of modern open-hole log interpretation. PennWell Publishing Company. Tulsa, Oklahoma.

Gerhard, J., & Alisan, C. (1987). Palynostratigraphy, paleoecology, and visual organic geochemistry Turgutbey-2, Değirmencik-3 and Pancarköy-1, Thrace Basin, Turkey. Turkiye Petrolleri Anonim Ortakligi Arastirma Merkezi Grubu Rapor No:983. p. 33. Ankara (unpublished).

Gorur, N., & Okay, A. I. (1996). A fore-arc origin for the Thrace Basin, NW Turkey. Geologische Rundschau, v. 85(4), p. 662–668.

Huvaz, O., Karahanoglu, N., & Ediger, V. (2007). The thermal gradient of the Thrace Basin, NW Turkey: correlation with basin evolution processes. Journal of Petroleum Geology, v. 30(1), p. 3–24.

Kasar, S., & Eren, A. (1986). Kırklareli-Saray-Kıyıköy bölgesinin jeolojisi. Turkiye Petrolleri Anonim Ortakligi Arama Grubu Rapor No:2208. p. 45. Ankara (unpublished).

Larionov, V. (1969). Borehole radiometry. Nedra, Moscow.

Perincek, D., Atas, N., Karatut, S., & Erensoy, E. (2015). Geological Factors Controlling Potential of Lignite Beds within the Danismen Formation in the Thrace Basin. Bulletin of the Mineral Research and Exploration, v. 150, p. 77–108.

Pickett, G. R. (1966). A review of current techniques for determination of water saturation from logs. Journal of Petroleum Technology, v. 18(11), p. 1425–1433.

Pickett, G. R. (1973). Pattern recognition as a means of formation evaluation. Society of Professional Well Log Analysts, 14th Annual Logging Symposium, Transactions, Paper A.

Sakınc, M., Yaltirak, C., & Oktay, F. Y. (1999). Palaeogeographical evolution of the Thrace Neogene Basin and the Tethys – Paratethys relations at northwestern Turkey (Thrace). Palaeogeography, Palaeoclimatology, Palaeoecology, v. 153, p. 17–40.

Sarac, G. (1987). Kuzey Trakya bölgesinde Edirne-Kirklareli, Saray-Çorlu, Uzunköprü-Dereikebir yöresinin memeli paleofaunasi. Ankara University.

Siyako, M., & Huvaz, O. (2007). Eocene stratigraphic evolution of the Thrace Basin, Turkey. Sedimentary Geology, v. 198(1–2), p. 75–91.

Steiber, S. J. (1970) Pulsed neutron capture log evaluation in the Louisiana Gulf Coast. Society of Petroleum Engineers, 45th Annual Meeting, paper SPE-2961.

Turgut, S., & Eseller, G. (2000). Sequence stratigraphy, tectonics and depositional history in eastern Thrace Basin, NW Turkey. Marine and Petroleum Geology, v. 17(1), p. 61–100.

Yilmaz, Y., Genc, S. C., Yigitbas, E., Bozcu, M., & Yilmaz, K. (1995). Geological Evolution of the Late Mesozoic Continental-Margin of Northwestern Anatolia. Tectonophysics, v. 243(1–2), p. 155–171.